LIGHTWEIGHT BUILDING CONSTRUCTION WITH LOCALLY AVAILABLE MATERIALS

By

Weisheng Hong

A THESIS

Submitted to
Michigan State University
in partial fulfillment of the requirements
for the degree of

Civil Engineering—Master of Science

2017

ABSTRACT

LIGHTWEIGHT BUILDING CONSTRUCTION WITH LOCALLY AVAILABLE MATERIALS

By

Weisheng Hong

Aerated slurry-infiltrated chicken mesh was evaluated as a lightweight and structurally resilient material for building construction. Aerated slurry with relatively low structural qualities was shown to perform favorably when used as a matrix with chicken mesh reinforcement in structural applications. The high specific surface area of chicken mesh and the close spacing of its wires (when used at 2-4% volume fraction) effectively enhance the mechanical performance and dimensional stability of the aerated slurry. The chicken mesh structural behavior also benefits significantly from embedment in the aerated slurry which mitigates the reorientation tendency of the chicken mesh wires under tension. This effect enables mobilization of the tensile load-carrying capacity of the wires in chicken mesh at structurally viable deformations.

A comprehensive experimental program was undertaken at materials and structures levels in order to develop aerated slurry-infiltrated chicken mesh materials and structural systems with a desired balance of strength, ductility and hysteretic energy dissipation capacity. The bulk density of the aerated slurry and the chicken mesh volume fraction were some key variables in design of the new (composite) building material. With proper selection of these variables, the synergistic actions of the aerated slurry and the chicken mesh in the context of the composite material were confirmed. Empirical models were developed for the mechanical performance of this composite material.

The aerated slurry-infiltrated chicken mesh composite material is amenable to joining via screw and (to some extent) nail application. An experimental study was conducted in order to evaluate the

effects of screw (or nail) type and geometric attributes as well as the aerated slurry-infiltrated chicken mesh bulk density and reinforcement condition on the pullout and (unilateral and cyclic) lateral behavior of screws and nails applied to aerated slurry-infiltrated chicken mesh sheets.

The combination of experimental data produced on structural elements, joints and joined components were used to design a building structure for efficient and safe performance under gravity and seismic loads. The full-scale building system is currently under construction for verifying its structural performance through shaking table tests.

ACKNOWLEDGMENTS

I would like to express my greatest gratitude towards my advisor, Dr. Parviz Soroushian, Professor of Civil Engineering and Environmental at Michigan State University. With his help, I gained much valuable knowledge. With his patience, support, encouragement and guidance, I could successfully complete my dissertation research project and graduate studies. With his support, I learned how to be a good scientist.

I would also like to appreciate Professor Roozbeh Dargazany and Professor Weiyi Lu for joining my guidance committee, and providing me with valuable help towards completing my dissertation research project.

I would like to thank fellow research group members, Areej Almalkawi and Mohammad Al-Orfi for their support and helpful suggestions. During my research project, they helped me overcome significant difficulties. I would not have been able to conduct my research project if they had not helped me with developing the required technical background and skills.

Additionally, I also would like to thank all the faculty members in the department of Civil and Environmental Engineering Department at Michigan State University, and all my fellow graduate students. I thank them for their help and support both in my research project and in my graduate coursework. I met many people during my time at MSU who helped me grow, and were willing to listen as I worked through both research and life problems.

Finally, I would also like to thank my family for their unconditional love and support throughout my academic life. Both my mother and father have been constant sources of encouragement throughout my life.

TABLE OF CONTENTS

LIST OF TABLES

LIST OF FIGURES

CHAPTER 1
INTRODUCTION

1.1. General

The goal of this research was to develop building structural materials and systems that can make effective use of locally available materials and construction resources. The building structure that evolved through this research program is now under construction for verification of its constructability and seismic performance via shaking table tests.

Aerated concrete with bulk densities less than 1 g/cm^3 is generally viewed as a non-structural material that offers thermal insulation qualities. It was found in this research investigation that a reinforcement system with high specific surface area, close spacing and desired mechanical bonding with matrix would enable use of aerated concrete in structural applications. Chicken mesh (poultry netting) was used in this investigation as a commonly available reinforcement that meets the requirements for transforming aerated concrete into a structural material. Viable volume (and area) fractions of chicken mesh for structural applications produce a high degree of congestion with the formwork. Therefore, an aerated slurry of high flowability was used to thoroughly infiltrate the congested reinforcement system, facilitating thorough consolidation and desired interfacial interactions. The mesh behaves as a homogeneous reinforcement to produce lightweight cementitious composites with a desired balance of strength-to-weight ratio, ductility and toughness (Wafa and Fukuzawa 2010). Ferrocement, a cementitious mortar with wire mesh reinforcement, provided the inspiration for development of aerated slurry-infiltrated chicken mesh (Naaman 2000).

1.2. Summary of Research

This thesis is divided into six chapters, with Chapters 1 through 5 prepared as a stand-alone paper written for submission to a scientific journal. A sixth chapter is devoted to structural design of the building system. For convenience, the references from each chapter have been consolidated and appear at the end of this thesis. A brief review of each chapter is presented below.

1.2.1. Mechanical Properties of Aerated Slurry-Infiltrated Chicken Mesh

Aerated slurry-infiltrated chicken mesh was evaluated as a ductile and lightweight material for building construction. The compressive strength of the aerated slurry, and the tensile, co pressive and flexural behavior of the aerated slurry-infiltrated chicken mesh were evaluated. The system exhibited a ductile failure mode which can be attributed to the high specific surface area and the desired mechanical interlocking of the chicken mesh reinforcement. The presence of chicken mesh was found to significantly alter the compressive strength of the aerated slurry. The effects of aeration on the system behavior were evaluated. A theoretical basis was developed for evaluating the mechanical behavior of aerated slurry-infiltrated chicken mesh.

1.2.2. Screw and Nail Behavior in Aerated Slurry-Infiltrated Chicken Mesh

Aerated slurry-infiltrated chicken mesh is developed as a lightweight building material which offers some key features of wood construction in terms of ease of construction, combined with the desired moisture resistance and durability characteristics of concrete. The aerated slurry-infiltrated chicken mesh building components can be joined using nails or preferably screws. An experimental investigation was conducted on the pullout as well as the unilateral and cycled lateral behavior of nails and screws applied to aerated slurry-infiltrated chicken mesh. These attributes of nails and screws strongly impact the structural behavior of building systems subjected to gravity and lateral (including seismic) forces. It was found that the interactions between nails or screws and the chicken mesh reinforcement in aerated slurry provides the screws or nails with desired lateral load-bearing capacity, ductility, and hysteretic energy absorption capacity. The nails and screws applied to aerated slurry-infiltrated chicken mesh also exhibited desired pullout behavior.

1.2.3. Behavior of a Lightweight Frame Made with Aerated Slurry-Infiltrated Chicken Mesh Under Cyclic Lateral Loading

Aerated slurry-infiltrated chicken mesh is a ductile and light-weight material for seismic-resistant building construction. An aerated slurry-infiltrated chicken mesh frame was subjected to cyclic lateral loading in order to assess its load-bearing capacity, ductility and hysteretic energy dissipation capacity. The frame exhibited a ductile failure mode compatible with its strong column-weak beam design. It also exhibited a desirable hysteretic energy dissipation capacity. Comparisons were made between the performance characteristics of this frame versus those of structural systems of similar geometric attributes made primarily of wood-based sheets. Semi-empirical models were developed for prediction of the structural behavior of aerated slurry-infiltrated chicken mesh. The structural performance of the frame made with aerated slurry-infiltrated chicken mesh under cyclic lateral loads was compared against those of lateral load-resisting systems of comparable geometric attributes comprising primarily of OSB and hardwood sheets.

1.2.4. Structural Evaluation of a Lightweight Building System Made with Locally Available Materials

Aerated slurry-infiltrated chicken mesh was evaluated as a lightweight structural material for building construction. The building system comprises frames and sheets, all of which contribute towards resisting gravity and lateral loads. Structural joining of the building components involves application of screws. Experimental investigations were undertaken to evaluate the performance of aerated slurry-infiltrated chicken mesh frame elements (beams and columns) and sheets under different force systems (bending moment, shear, punching shear, compression). A scaled structural subcomponent comprising aerated slurry-infiltrated chicken mesh frames to which sheets were screwed was also tested under cyclic lateral loads. Structural analysis methods were developed for aerated slurry-infiltrated chicken mesh.

1.2.5. Structural Design of a Lightweight Building System Made with Locally Available Materials

The design loads of aerated slurry-infiltrated chicken mesh buildings were decided. The critical factored load combinations were identified. The aerated slurry-infiltrated chicken mesh frames, wall and roof/ceiling sheets and floor panels, and screws joining the sheets to building frames were designed to safely resist the governing load combinations.

1.2.6. Durability Characteristics of Aerated Slurry-Infiltraetd Chicken Mesh

The effects of accelerated weathering on the flexural performance of aerated slurry-infiltrated chicken mesh sheets were evaluated. This lightweight building material has been developed for convenient construction of affordable, safe and energy-efficient buildings using locally available materials and resources. External sheets that envelope the building are subjected to weathering exposure. Investigations were performed on the effects of accelerated weathering on the flexural performance of aerated slurry-infiltrated chicken mesh sheets. Standard methods of accelerated aging developed for cementitious siding and roofing sheets were followed. Two test methods involving exposure of sheets to wetting-drying and freezing-thawing cycles were implemented. Aerated slurry-infiltrated chicken mesh sheets were found to perform desirably under these accelerated aging effects.

CHAPTER 2
MECHANICAL PROPERTIES OF AERATED SLURRY-INFILTRATED CHICKEN MESH

2.1. Introduction

Aerated concrete is traditionally viewed as an insulating (non-structural) building material. A primary premise of the work reported herein is that a reinforcement system with high specific surface area and desired mechanical bonding within matrix would enable use of aerated concrete in structural applications. There is a growing interest in the use of wire mesh reinforcement in concrete panels. Within certain limits, the mesh behaves as homogeneous reinforcement, and produces concrete composites with highly desired tensile strength-to-weight ratio, cracking behavior and impact resistance(Wafa and Fukuzawa 2010). Ferrocement, a cementitious mortar with wire mesh reinforcement, benefits from these advantages associated with the use of nearly isotropic reinforcement systems of high specific surface area and desired mechanical bonding (Naaman 2000).

Chicken mesh (poultry netting) was used as a readily available reinforcement system of high specific surface area with desired mechanical bonding potential in aerated slurry. Viable volume (and area) fractions of chicken mesh for structural applications produce a high degree of congestion with the formwork. Therefore, an aerated slurry of high flowability was used to thoroughly infiltrate the congested reinforcement system, facilitating thorough consolidation and desired interfacial interactions.

Streamlined methods were devised for producing aerated slurry-infiltrated chicken mesh as a structural material. An experimental program was conducted in order to gain insight into the mechanical performance of this material. The effects of chicken mesh reinforcement on the compressive strength of aerated slurry was investigated. The effect of aeration of slurry on the system performance was also evaluated. A semi-empirical theoretical basis was developed for the mechanical behavior of aerated slurry-infiltrated chicken mesh.

2.2. Experimental Program

2.2.1. Materials

2.2.1.1. Aerated Slurry

The slurry mix was prepared in this investigation with Type I Portland cement and tap water. In one of the mixtures, in order to achieve a viable fresh mix workability, a polycarboxylate-based superplasticizer was used. The aerated slurry was prepared by adding a foaming agent to the mixing water of slurry. Aeration introduces a homogenous system of fine air bubbles into the cement paste. This is accomplished using foaming agents that stabilize the air voids generated by agitating the mixing water of slurry to which the foaming agent has been added (Nambiar and Ramamurthy 2007, Ramamurthy, Nambiar et al. 2009, Zhang, Provis et al. 2014). Preparation of the aerated slurry started with production of foamed water. For this purpose, a foaming agent extracted from plants (saponin) was blended with the mixing water at 1200 rpm rotational speed using a mixing blade attached to a drill (Figure 1). The resulting foamed water was then added to cement, and mixed in a mortar mixer for 6 minutes.

(a) Prior to stirring (b) Foaming after stirring

Figure 1. Preparation of foamed water by stirring the mixing water incorporating the foaming agent.

2.2.1.2. <u>Chicken Mesh</u>

This work chose chicken mesh (hexagonal 20-gauge galvanized poultry netting) as a steel reinforcement system of high specific surface area. This selection was made due to the broad worldwide availability of chicken mesh. The common mesh used in this investigation was made of steel wires of 1 mm diameter (0.785 mm^2 cross sectional area). Chicken meshes are available with different wire diameters and spacings. The spacing of hexagonally configured wires generally increase with increasing wire diameter in order to provide comparable wire cross-sectional areas per unit width. Given the relatively large layers of chicken mesh that need to be infiltrated with aerated slurry, the preference in this investigation was for chicken meshes with larger wire diameter and spacing. The chicken mesh used in this investigation was non-isotropic. The stronger direction (vertical in Figure 2) is referred to as longitudinal in this work.

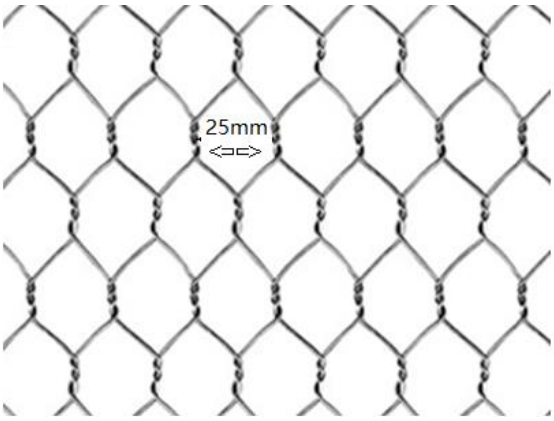

Figure 2. The chicken mesh used in the experimental program.

2.2.2. Experimental Methods

An experimental program was conducted in order to evaluate the effects of some key variables on the mechanical properties of aerated slurry-infiltrated chicken mesh under compressive, flexural and tensile loading. The interactions of chicken mesh with aerated slurry can be characterized as more complex than those between concrete and conventional reinforcing bars. More attention should be paid to the contributions of the aerated (slurry) matrix towards timely mobilization of the load-bearing capacity of the multiple chicken mesh layers tightly incorporated into the aerated slurry. Test results would be critical to understanding these complex interactions. Aerated slurry-infiltrated chicken mesh can, due to the high specific surface area of steel reinforcement, provide distinctly high levels of ductility and energy dissipation capacity. In addition, the high specific surface area and close spacing of chicken mesh wires could benefit various aspects of the aerated slurry performance, including its compressive strength, dimensional stability and resistance to shrinkage cracking. The experimental methods used for evaluating the mechanical behavior of aerated slurry-infiltrated chicken mesh are presented in the following. The experimental were used to develop semi-empirical models for predicting the mechanical performance of aerated slurry-infiltrated chicken mesh.

2.2.2.1. <u>Tests performed on slurry without chicken mesh reinforcement</u>

The experimental work reported here used one non-aerated slurry as control, and different aerated slurry mixtures. The non-aerated slurry comprised cement: water: superplasticizer at 1: 0.36: 0.004 weight ratios. For the purpose of preparing the aerated slurry mixtures, the foaming agent was added to water and subjected to stirring at relatively high speed in order to product foamed mixing water, which was then added to cement and mixed using normal mixing procedures. The water/cement ratio of aerated slurry mixtures ranged from 0.40 to 0.55. The aerated slurry mix proportions are introduced in Table 1 The resulting aerated slurry was placed in 50 mm cube molds for compression strength test and bulk density measurement. The specimens kept in sealed condition at room temperature for 24 hour and cured at 95% relative humidity and room temperature for 7 days.

Table 1. The aerated slurry mix proportions.

Mix	*Foaming Agent Dosage, % by wt.*	*Water/cement ratio*
0	*0*	*0.35 with 0.004 superplasticizer*
1	0.005%	0.45
2	0.01%	
3	0.02%	
4	0.005%	0.50
5	0.01%	
6	0.02%	
7	0.005%	0.55
8	0.01%	
9	0.015%	
10	0.02%	
11	0.025%	
12	0.03%	
13	0.02%	0.6
14	0.025%	

2.2.2.2. <u>Tests performed on aerated slurry-infiltrated chicken mesh</u>

The prismatic compression test specimens had planar dimensions of 102 mm by 102 mm, with a height of 229 mm. The chicken mesh configuration used in compression testing of aerated slurry-infiltrated chicken mesh specimens is presented in Figure *3*. There were two groups of chicken mesh in these specimens: (i) 30 interior layers placed in folded form; and (ii) four exterior layers wrapped around the interior layers to mitigate the potential for split cracking upon screw application to the surface. Along the height, where the chicken mesh layers are oriented in their strong direction, the total number of chicken mesh layers is thus 38. The aerated slurry mixture comprised cement: water: saponin at 1: 0.6: 0.00045 weight ratios.

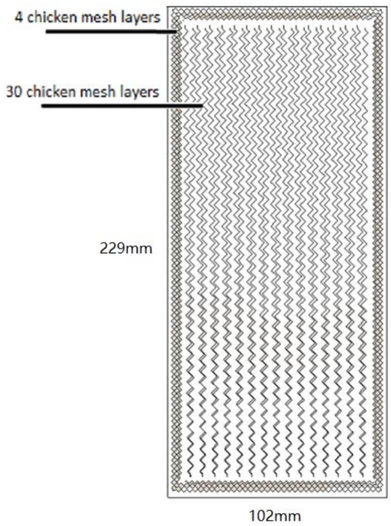

Figure 3. Aerated slurry-infiltrated chicken mesh compression test specimen.

Aerated slurry0infiltrated chicken mesh sheets with 20 mm thickness and 150 mm width were subjected to tension testing. The number of chicken mesh layers in different tension test specimens varied from 12 to 24. The chicken mesh layers were oriented to that the tensile force was resisted in their strong direction. The tension test setup is shown in Figure *4*. The free length of the tension test specimen between the two grips was 310 mm (with a total specimen length of 500 mm). Tension tests were performed at a constant displacement rate of 0.05 mm/s. The values of load and deflection were recorded during the tension tests using a data acquisition system.

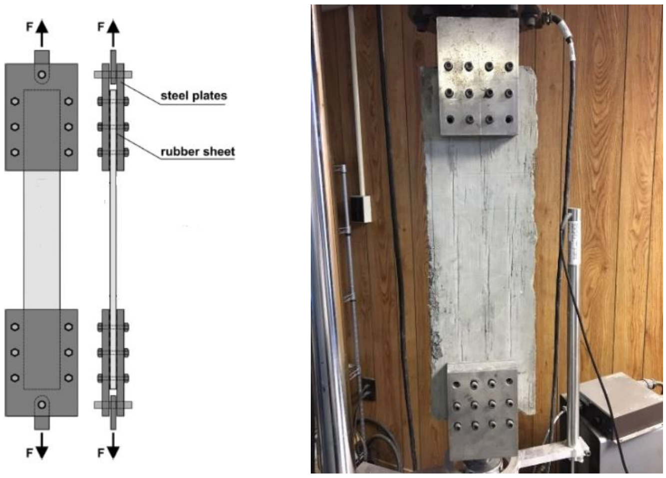

Figure 4. Tension test setup.

The aerated slurry-infiltrated chicken mesh sheets tested in flexural had the same dimensions as the tension test specimens. They were subjected to four-point flexure loading over a span of 450 mm. Load was applied quasi-statically (with a constant displacement rate of 0.033 mm/s), and load-deflection data were collected during the flexure test up to failure.

Figure 5. Flexure test setup.

2.3. Test Results and Discussion

2.3.1. Compressive strength and bulk density of aerated slurry

The aerated slurry mix designs, defined by the foaming agent dosage (expressed as wt.% of cement) and water/cement ratio, were presented in Table 1. The measured values of 7-day compressive strength and bulk density are presented in Table *2* and Figure *7*. Lower values of bulk density tend to correspond with lower compressive strength values. This is both because of the rise in air content and also the increase in water/cement ratio at higher dosages of foaming agent for achieving viable fresh mix rheology. Mix #13 with density of 0.9 g/cm^3 and compressive strength of 5.4 MPa at 7 days provides a viable balance of bulk density and strength for the targeted application. When compared with non-aerated slurry, it can be noted that aeration of slurry (Mix #13) produced 61% drop in bulk density and 90% drop in compressive strength. This work emphasized reduction of density in order to limit seismic forces (Guo, Juan et al. 2011, Ohsaki, Miyamura et al. 2016) and also allow for manual installation of the building structural components. It was hypothesized that the presence of closely spaced chicken mesh wires with high specific surface area would benefit the compressive strength of aerated slurry-infiltrated chicken mesh.

Table 2. Compressive strength and bulk density of different aerated slurry mixtures (Mix 0 is non-aerated).

Mix	7-Day Compressive Strength, MPa	Bulk Density, g/cm^3
0	50	2.2
1	10.7	1.9
2	8.2	1.5
3	6.3	1.4
4	14.1	1.2
5	10.5	1.81
6	9.2	1.3
7	13.3	1.6
8	11.1	1.7
9	9.4	1.3
10	6.4	1.17
11	2.4	0.65
12	1.2	0.8
13	5.4	0.9
14	7.1	1.12

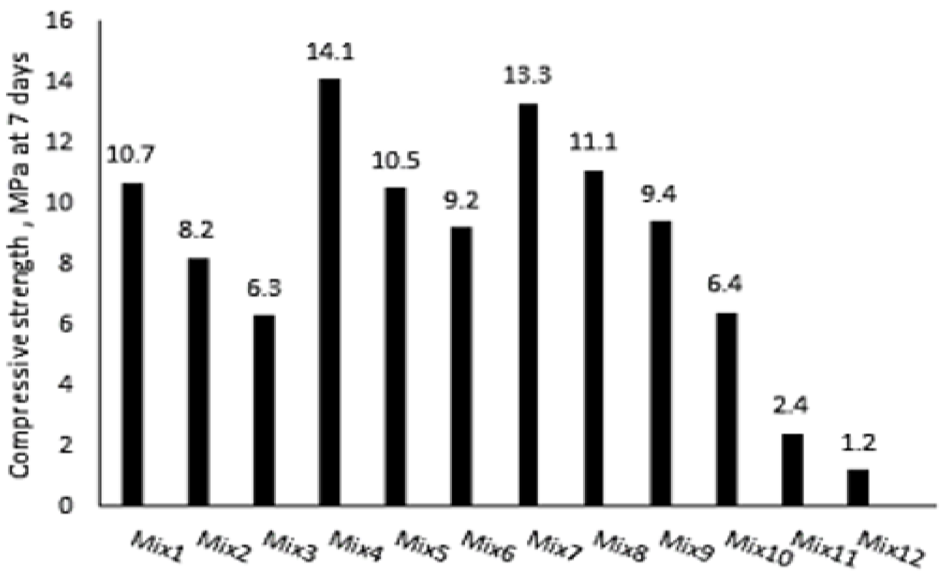

(a). Compressive strength and bulk density test results for different aerated slurries.

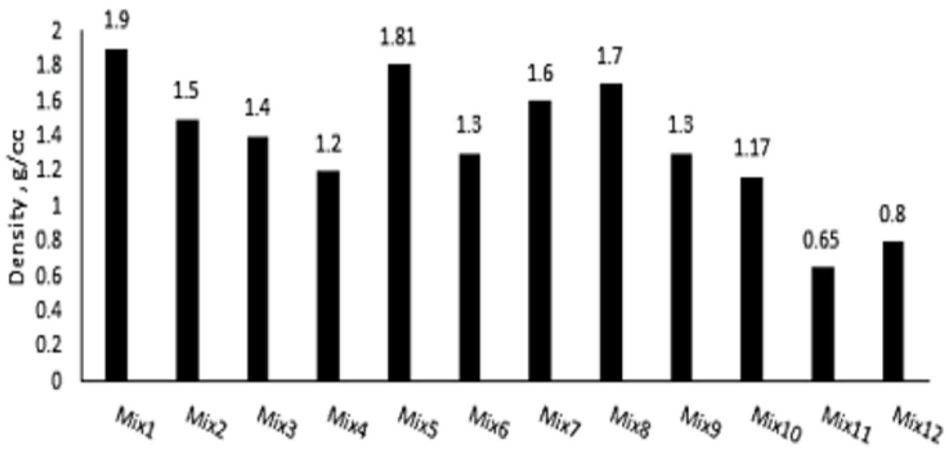

(b). Compressive strength and bulk density test results for different aerated slurries.

Figure 6. Compressive strength and bulk density test results for different aerated slurries.

2.3.2 Compressive behavior of the aerated slurry-infiltrated chicken mesh

A typical compressive stress-deflection curve for an aerated slurry-infiltrated chicken mesh prepared with the aerated slurry Mix #13 is presented in Figure *7*. The presence of chicken mesh significantly improved the compressive strength and ductility of the aerated slurry. The aerated slurry alone provided a compressive strength of 5.4 MPa. In the presence of chicken mesh, a strain-hardening behavior was observed after this strength levels was reached. The ultimate strength was more than

15 MPa, noting that the specimen was unloaded after the maximum deflection limit of the test system was reached at about 70 mm. One can attribute the observed strain-hardening behavior (and the corresponding rise in compressive strength) of the aerated slurry-infiltrated chicken mesh partly to the confining effect rendered by the wire mesh with closely spaced wires of high specific surface area.

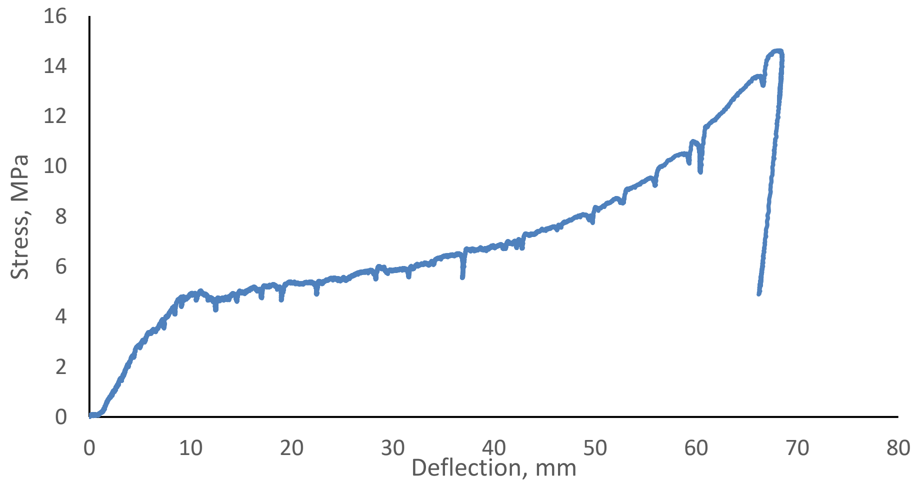

Figure 7. A typical compressive stress-deflection behavior of aerated slurry-infiltrated chicken mesh.

2.3.3 Tensile behavior of aerated slurry-infiltrated chicken mesh

The three slurries considered in this experimental program provided bulk densities (after hardening and air-drying) of: (1) 2.2 g/cm^3; (2) 1.3 g/cm^3; and (3) 0.8 g/cm^3. The highest density of 2.2 g/cm^3 was obtained without aeration of slurry. The tensile load-deflection curves obtained with 18 layers of chicken infiltrated with aerated (or non-aerated) slurry (producing a sheet of 25 mm thickness) are presented in Figure *8* together with the load-deflection curve for 18 layers of chicken mesh obtained without slurry-infiltration. The corresponding tensile stress-deflection curves for slurry-infiltrated chicken mesh specimens are presented in Figure 10. Slurry infiltration is observed in Figure *8* to significantly raise the stress levels (within the 0-30 mm deflection range considered here) of chicken mesh layers. The misaligned configuration of chicken mesh wires make it significantly compromises its stiffness and thus its merits as a tensile load-bearing system. The tendency towards realignment of chicken mesh wires at small deflections seriously undermine its structural stiffness. Infiltration with slurry (including aerated slurry), on the other hand, resists this tendency woards realignment of wires, and thus enables mobilization of the tensile load-carrying capacity of the chicken mesh wires at relatively small displacements. Aeration of the slurry to reduce its bulk density does not significantly undermine its ability to mobilize the chicken mesh wires at small displacements to resist tensile forces. In short, chicken mesh and aerated slurry exhibit synergistic effects in the context of aerated slurry-infiltrated chicken mesh. The confining effects of chicken mesh increases the compressive strength of aerated slurry by more than 200%. Infiltration of chicken mesh with slurry also enables effects use of the tensile load-carrying capacity of the chicken mesh wires at structurally viable deformation levels.

Reduction of the slurry density via aeration from 2.2 to 0.8 g/cm^3 (by 63%) lowered the tensile strength of aerated slurry infiltrated chicken mesh from 5.4 to 4.2 MPa (by only 22%), as shown in Figure *9*. This finding points at the potential of the aerated slurry-infiltrated chicken mesh to provide a desired balance of low bulk density and relatively high tensile strength. The tensile stiffness of slurry-infiltrated chicken mesh was not reduced significantly upon aeration for lowering its bulk density.

Figure *10* shows a tensile specimen of aerated slurry-infiltrated chicken mesh after failure in tension. A distributed damage zone was observed where the tendency towards realignment of chicken mesh wires, that was resisted by the aerated slurry surrounding the wires, led to crushing of the aerated slurry at large deformations.

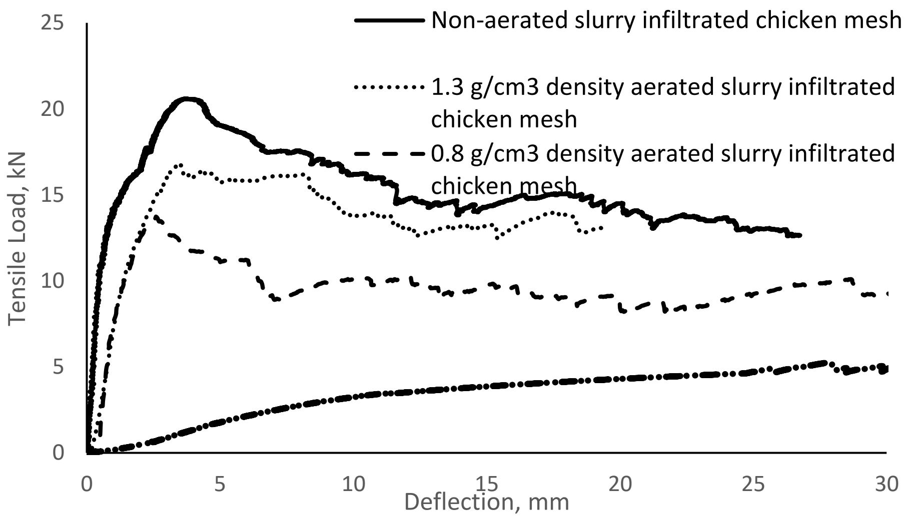

Figure 8. Tensile load-deflection curves for non-aerated and aerated slurry-infiltrated chicken mesh, and also for chicken mesh tested alone (without slurry-infiltration).

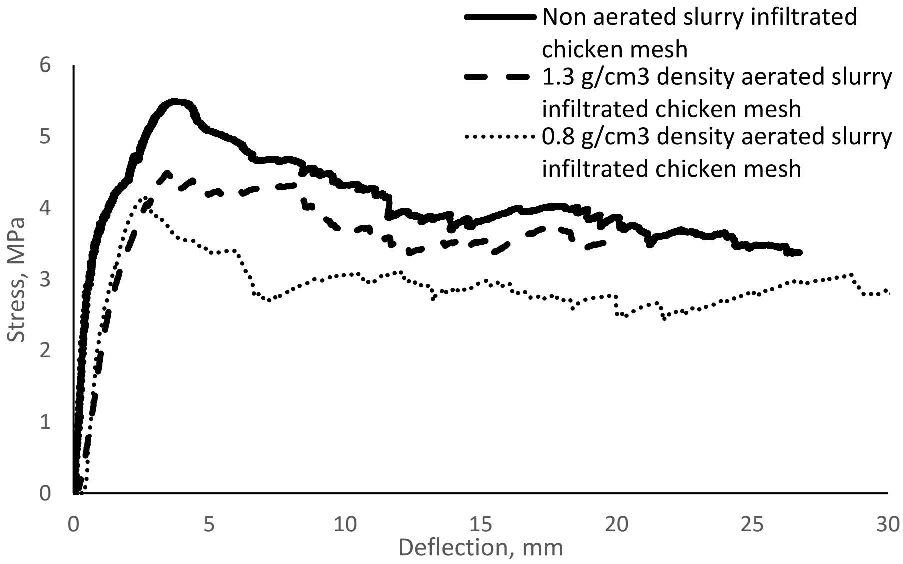

Figure 9. Tensile stress-deflection curves for non-aerated and aerated slurry-infiltrated chicken mesh.

Figure 10. Typical appearance of a failed tension test specimen of aerated slurry-infiltrated chicken mesh at relatively large tensile deformations.

The tensile strengths obtained for the slurry-infiltrated chicken mesh sheets presented above are summarized in Table *3*. While the slurry density and the number of chicken mesh layers influence the tensile strength of aerated slurry-infiltrated chicken mesh sheets (with high concentration of chicken mesh), all these tensile strengths (except when 6 or 9 layers of chicken mesh are used) occur within a relatively narrow 3.64 – 4.40 MPa range. Significant reduction of bulk density could be obtained via aeration of the slurry without significant loss of the slurry-infiltrated chicken mesh tensile strength. These observations point at the potential of aerated slurry-infiltrated chicken mesh to provide a desired balance of tensile strength and bulk density.

Table 3. A summary presentation of the tensile strength test results for slurry-infiltrated chicken mesh sheets with different slurry densities and number of chicken mesh layers.

Slurry	Chicken Mesh Layers	Saponin/Cement (weight ratio)	Water/Cement (weight ratio)	Bulk Density (g/cm^3)	Tensile Strength (MPa)
Non-Aerated	18/24	-	0.36* (0.004 superplasticizer)	2.2	5.48/ 5.60
Aerated	16/18	0.0002	0.5	1.3	3.71/ 4.40
Aerated	6/9/12/ 18	0.0005	0.6	0.8	1.67/2.65/3.64/4.20

Superplasticizer at 0.004 by weight of cement

2.3.4 Flexural performance

The three slurries considered in this experimental program provided bulk densities (after hardening and air-drying) of: (1) 2.2 g/cm^3; (2) 1.3 g/cm^3; and (3) 0.8 g/cm^3. The highest density of 2.2 g/cm^3 was obtained without aeration of slurry. Typical flexural stress-deflection curves for sheets of 25 mm thickness made with non-aerated and aerated slurries using 18 layers of chicken mesh are presented in Figure *11*. The flexural behavior is observed to be ductile. Aeration of slurry lowered the flexural strength but not the ductility of the aerated slurry-infiltrated chicken mesh. Increasing the dosage of foaming agent to reduce the bulk density of the aerated slurry from 1.3 to 0.8 g/cm^3 had relatively small effects on the flexural performance of the resultant sheets. The peak flexural stress obtained with aerated slurry of 0.8 g/cm^3 bulk density was 6.9 MPa. Reduction of the aerated slurry density from 1.3 to 0.8 (by 38%) led to a reduction of the flexural stress from 7.8 MPa to 6.9 MPa (by 11%). The flexure test specimens prepared with non-aerated slurry exhibited multiple cracking and a distributed flexural failure mode (Figure *12*a); flexural failure of the aerated specimens was less distributed (Figure *12*).

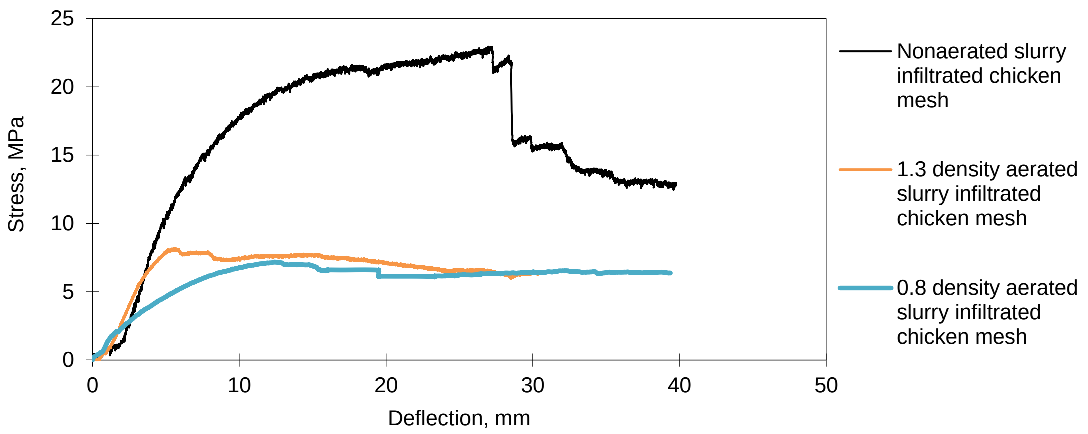

Figure 11. Flexure stress-deflection curves for non-aerated and aerated slurry-infiltrated chicken mesh sheets.

(a) Non-aerated slurry (b) Aerated slurry

Figure 12. Flexural failure modes of non-aerated and aerated slurry-infiltrated chicken mesh sheets.

2.3.5 Analysis of aerated slurry-infiltrated chicken mesh

The aerated slurry makes significant indirect contributions toward tensile strength by restraining the chicken mesh wires (which are partly oriented at an angle with respect to the tensile stress siewxrion) from reorientation under tensile stress. The tensile strength of aerated slurry-infiltrated chicken mesh was expressed as follows:

$$\sigma_T = \alpha \rho f_y$$

where, σ_T = tensile strength of the aerated slurry infiltrated chicken mesh, ρ = area ratio of the chicken mesh wires, f_y = yield stress of the chicken mesh wires (310 MPa), and α = an empirical efficiency factor which reflects the degree of restraint offered by the aerated slurry against reorientation of the chicken mesh layers as well as the orientations of wires with respect to the tensile stress direction. An average value of α = 0.26 allows for prediction of the experimental values of tensile strength using the above equation.

In compression, one should account for the direct contribution of the chicken mesh wires (embedded in the aerated slurry matrix), and also their indirect confining effect which raises the effective compressive strength of the slurry. Considering these contributions of chicken mesh, the composite compressive strength of aerated slurry-infiltrated chicken mesh may be expressed as follows:

$$\sigma_C = \beta \rho f_y + \gamma f_c'$$

where, σ_c = compressive strength of the aerated slurry-infiltrated chicken mesh, β = efficiency factor for the chicken mesh reinforcement in compression (it was assumed to be similar to the empirically derived efficiency factor of chicken mesh in tension, that is 0.26), and γ = efficiency factor of the aerated sully in compression, which benefits from the confining effect of the chicken mesh reinforcement. A γ value of 4.6 allowed the above equation to predict the compression test results performed on aerated slurry-infiltrated chicken mesh. In other words, the aerated slurry that benefits from the beneficial effects of chicken mesh provides 4.6 times the compressive strength of plain aerated slurry. These relatively large beneficial effects can be attributed to: (i) the relatively low elastic modulus and high Poisson's ratio of the aerated slurry that produce relatively large strains in compression which, are restrained by the chicken mesh reinforcement of high elastic modulus and specific surface area with closely spaced wires, resulting in confining effects which raise the aerated slurry compressive strength; (ii) chicken mesh with high specific surface area and close wire spacing effectively reinforces the aerated slurry against the microcrack formation under restrained shrinkage, and the growth of these microcracks under load. The rise in compressive strength of aerated slurry with chicken mesh reinforcement is a significant factor enabling the otherwise non-structural (insulating) aerated slurry to make contributions to the aerated slurry-infiltrated chicken mesh structural performance.

Using concepts similar to those used with reinforced concrete, the nominal flexural strength (M_n) of an aerated slurry-infiltrated chicken mesh cross-section (Figure 13) can be expressed as follows:

$$M_n = \alpha \rho f_y b(h-a)(\frac{h}{2})$$

where, 'a' is a value related to (and somewhat smaller than) the depth of neutral axis (c), and b and h are, respectively, the width and height of a rectangular cross-section. Similar to the approach to reinforced concrete flexural analysis, a constant compressive stress is assumed up to depth 'a' in order to simulate the nonlinear compressive stress distribution up to the depth neutral axis depth of 'c'. The value of 'a' can be derived based on the equilibrium of the tensile and compressive forces generated at the section under bending moment:

$$\alpha \rho f_y(h-a) = \left(\beta \rho f_y + \gamma f_c'\right)a$$

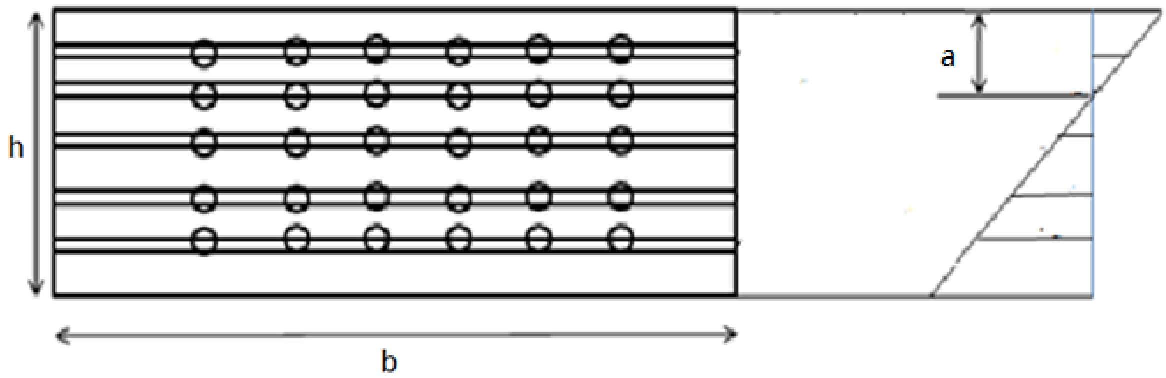

Figure 13. Cross-section and flexural strain distribution of an aerated slurry infiltrated chicken mesh rectangular section.

As a first step, the expression derived above for the nominal flexural strength of aerated slurry-infiltrated chicken mesh was verified using the experimental data generated for a beam and two sheets made with aerated slurry-infiltrated chicken mesh. These structural test specimens were made with a slurry proportioned at saponin: water: cement weight ratios of 0.00045: 0.6: 1 (which yielded a bulk specific gravity of 0.8 after hardening and air-drying). Table 4 presents the aerated slurry-infiltrated chicken mesh sheet dimensions, reinforcement conditions, test results, and the experimental and theoretical values of flexural strength. The theoretical values of flexural strength obtained with the expression presented above are observed to be less than experimental values by only 3 to 5%. The approach outlined above for calculation of the nominal flexural strength of aerated slurry-infiltrated chicken mesh sheets and beams thus yielded favorable accuracy based on the limited test data generated in this investigation.

Table 4. Aerated slurry-infiltrated chicken mesh sheet and beam dimensions, reinforcement and loading conditions, and test results versus predicted values.

Specimen	# of Chicken Mesh Layers	Span, mm	Width, mm	Thickness, mm	Reinf. Area Ratio	Density, g/cm^3	Peak Load, N	3 or 4 Point Loading	Flexural Strength, N.m	
									Test	Theory
Sheet	12	450	150	20	0.04	0.8	1300	4	97.5	92.67
Sheet	18	450	150	25	0.03	0.8	2500	4	180.5	170.41
Beam	30	800	102	254	0.02	0.8	25000	3	5000	4910.248

CHAPTER 3
SCREW AND NAIL BEHAVIOR IN AERATED SLURRY-INFILTRATED CHICKEN MESH

3.1. Introduction

Aerated concrete is traditionally viewed as an insulating (non-structural) building material. The work reported herein employs a readily available reinforcement system (chicken mesh) of high specific surface area and desired mechanical bonding with matrix to enable structural applications of aerated concrete. Within certain limits, the mesh behaves as homogeneous reinforcement, and produces lightweight cementitious composites with highly desired tensile strength-to-weight ratios, cracking behavior, ductility, toughness and impact resistance (Wafa and Fukuzawa 2010). Ferrocement, a cementitious mortar with wire mesh reinforcement, benefits from these advantages associated with the use of nearly isotropic reinforcement systems of high specific surface area and desired mechanical bonding (Naaman 2000). Aerated slurry-infiltrated chicken mesh differs from ferrocement by the aeration of the matrix for weight reduction, and use of a flowable slurry for infiltration of the slurry between the closely spaced wires of chicken mesh, noting that the relatively fine diameter of the chicken mesh wires (when compared with the mesh reinforcement commonly used in ferrocement) yields closer wire spacings.

Joining of the aerated slurry-infiltrated chicken mesh with screws or nails is an important factor in simplifying the construction process. Nail and screw behavior would strongly impact the structural performance (including seismic resistance) of aerated slurry-infiltrated chicken mesh building systems (ASTM 2012). The ductility and hysteretic energy absorption capacity of screws or nails in shear play an important role in dissipating the seismic energy input to the building (Rosowsky and Reinhold 1999, Ganne-Chedeville, Pizzi et al. 2005). The approach to seismic design of aerated slurry-infiltrated chicken mesh building systems emphasizes adequate strength and ductility of nails or screws in pullout and lateral behavior, and their ability to provide favorable hysteretic behavior for dissipating the input energy of earthquakes (Dolan and Madsen 1992, Herzog and Yeh 2006).

3.2. Material and Methods

3.2.1 Materials

Saponin was used as the foaming agent for production of aerated slurry. The saponin used in this investigation was obtained from plants. The work reported herein was performed using Type I Portland cement; other hydraulic cements could also be used in this application. The slurry used here had a water/cement ratio of 0.6; the saponin/cement ratios considered here were 0.0005 and 0.00035, which produced hardened material bulk densities of 0.78 g/cm^3 and 0.9 g/cm^3, respectively. The chicken mesh used in this investigation was hexagonal 20-gauge galvanized poultry netting (Figure 14). This commonly available mesh is made of steel wires of 1 mm diameter (with 0.785 mm^2 cross sectional area).

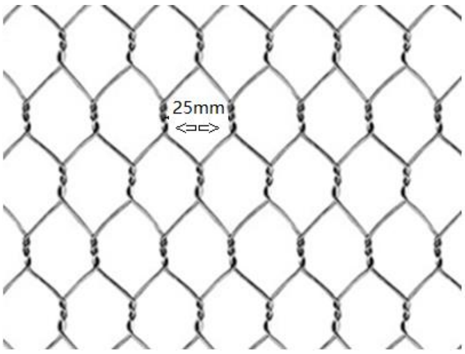

Figure 14. The chicken mesh used in the experimental program.

Three types of screw and two types of nail were considered in this test program (Figure 15). The screws were: (i) Philips bugle-head coarse thread sharp point polymer coated exterior screw (#10 x 4 in.) with 101.6 mm length and 4.19 mm diameter (Model # PTN4S1, for exterior use); (ii) Philips bugle-head coarse thread sharp point polymer coated exterior screw (#10 x 3-1/2 in.) with76.2 mm length and 3.5 mm diameter (Model # PTN312S1, for exterior use); and (iii) Philips zinc-plated flathead wood screws (#14 x 4 in.) with 101.6 mm length and 6.02mm (Model # 807791, for both interior and exterior use). The two nails were: (i) Common nail Model 20HGC1, for interior use (#6 x 4 in.) with 101.6 mm length with 4.19 mm diameter; and (ii) Pro-fit 010202ddeck nail (20D x 4 in), hot dip galvanized with 101.6 mm length and 4.19 mm diameter. These screws and nails were applied perpendicular to the plane of aerated slurry-infiltrated chicken mesh sheets.

(a) Screws (b) Nails

Figure 15. The screws and nails used in the test program

3.2.2 Test Methods

The screw and nail pullout test setup is shown in Figures 16. A servovalve-controlled hydraulic test system was used to pull a screw or nail out at a rate of 1.5 mm/min (ASTM 2012). A data acquisition system collected the load and deflection test data from a load cell and a displacement transducer throughout the pullout process. The aerated slurry-infiltrated chicken mesh sheets used in pullout tests were 80 mm thick with 300 mm by 300 mm planar dimensions. They were reinforced with 30 layers of chicken mesh. The slurry was simply poured onto the chicken mesh; it was fluid enough to thoroughly infiltrate the chicken mesh layers within the sheet thickness. Tests were performed after 7 days of moist curing (at room temperature) of the aerated slurry-infiltrated chicken mesh sheets.

Figure 16. The pullout test setup.

The test setup used for evaluating the monotonic lateral behavior of screws and nails acting against an aerated slurry-infiltrated chicken mesh sheet is shown in Figure 17. The sheet used for this purpose was 15 mm thick with 500 mm x 500 mm planar dimensions. It was reinforced with 12 layers of chicken mesh. Test were performed after moist curing of the sheets for 7 days at room temperature. The monotonic lateral tests were performed at a crosshead speed of 6 mm/min. The load-deflection behavior was monitored via collection of data using a a data acquisition system from load cell and a displacement transducer.

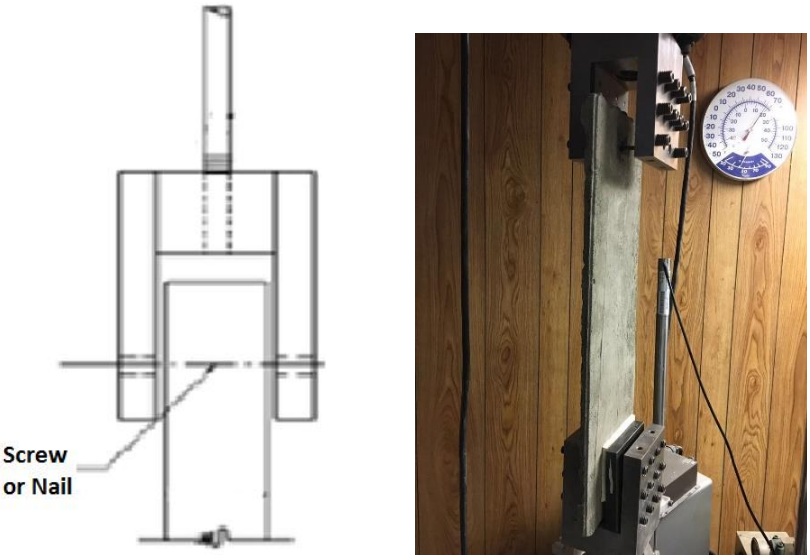

Figure 17. The test setup used for evaluation of the lateral behavior of a screw or nail in an aerated slurry-infiltrated chicken mesh sheet.

The cyclic lateral tests were performed two screws or nails applied in two configurations, as shown in Figure 18. In the first configuration (Figure 18a), the center of the first screw or nail was at 5 cm distance from the sheet edge, and the center-to-center spacing of the screws or nails was 5 cm. In the second configuration (Figure 18b), both screws or nails were centered at 5 cm from the sheet edge, and their center-to-center spacing was 7.5 cm.

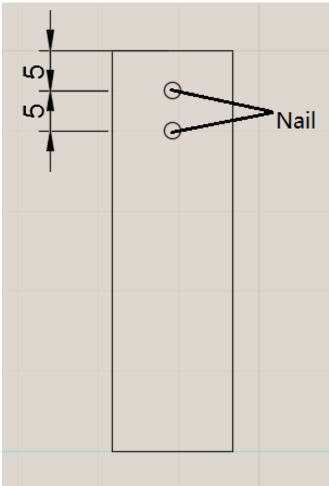

1. Screws or nails aligned parallel to the loading direction

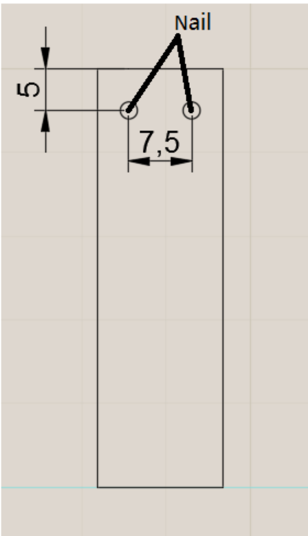

(b) Screws or nails aligned perpendicular to the loading direction

Figure 18. Nail configurations and test setups used in experimental evaluation of the lateral behavior of nails under cyclic loads

Cyclic tests were performed quasi-statically at a frequency of 0.09 Hz; the sine function used in this cyclic testing is shown in Figure 19 and summarized in Table 5. The four cycles marked 'stabilizing cycles' were used to achieve a stabilized hysteretic curve. A degradation of no more than 5% shall be present between successive cycles. If a larger degradation exists, tests shall be repeated with a higher number of cycles within this set (Dolan and Madsen 1992, Dolan 1994) in order to determine the level at which the performance stabilizes. This stabilized hysteresis curve is used to calculate the stabilized energy dissipation of the connection (Kazantzi and Vamvatsikos 2012), and provides conservative estimates of the performance parameters that would be expected in structures previously loaded or subjected to a large number of cycles during a loading event (Uang and Bertero 1990).

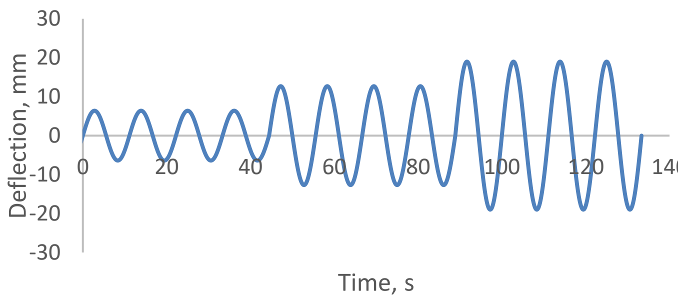

Figure 19. Time-displacement curve for cyclic tests

Table 5. The displacement cycles used in lateral testing of nails.

Number of Cycles	Maximum Displacement, mm	Displacement Rate (sine function)
4	±6.4 ±12.7 ±19.0	0.09 Hz

3.3. Test Results and Discussion

3.3.1 <u>Screw or Nail Pullout Behavior in Aerated Slurry-Infiltrated Chicken Mesh</u>

Figure 20 presents a typical pullout load-deflection behavior of the common nail introduced earlier from an aerated slurry-infiltrated chicken mesh sheet with 18 layers of chicken mesh (with 0.78 bulk specific gravity of aerated slurry). A peak pullout load of 183 N was obtained in this specific test. The nail pullout behavior is observed to be ductile.

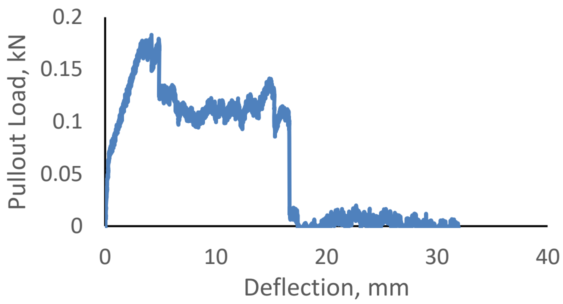

Figure 20. A typical common nail pullout load-deflection behavior.

The screw and nail pullout test data generated for different screw or nail sizes and sheet thicknesses/number of chicken mesh layers are summarized in Table 6. It was necessary to pre-drill a hole of smaller diameter prior to application of screw to aerated slurry-infiltrated chicken mesh the diameter of the (masonry) drill bits used for this purpose are presented in Table 6. In general, screws exhibited a better pullout performance than nails. The galvanized spiral nail produced a better pullout behavior than the common nail. The pullout behavior of nails and screws from aerated slurry-infiltrated chicken mesh benefited significantly from increasing the bulk density of the aerated slurry. Figure 21 shows a typical appearance of the aerated slurry-infiltrated chicken mesh sheet after pullout of a screw.

Table 6. Summary of the screw and nail pullout test results.

Nail or Screw Type	Bulk Density of the Aerated Slurry-Infiltrated Chicken Mesh, g/cm^3	Drill Bit Diameter, mm	Peak Pullout Force, N
Common nail of 101.6 mm length and 4.19 mm diameter	0.78	-	183
Common nail of 101.6 mm length and 4.19 mm diameter	0.90	-	365.5
Galvanized spiral nail of 101.6 mm length and 4.19 mm diameter	0.78	-	567.6
Exterior screw of 76.2 mm length and 3.5 mm diameter	0.78	3.17	1050
Exterior screw of 101.6 mm length and 4.19 mm diameter	0.78	3.17	1270
Zinc-coated wood screw of 101.6 mm length and 6.02 mm diameter	0.78	4.76	3080

Figure 21. Typical appearance of the aerated slurry-infiltrated chicken mesh sheet after pullout of a screw

3.3.2 <u>Screw or Nail Lateral Behavior in Aerated Slurry-Infiltrated Chicken Mesh Sheets</u>

Typical lateral load-deflection behavior of an exterior screw of 101.6 mm length and 4.19 mm diameter in aerated slurry-infiltrated chicken mesh with 0.78 g/cm^3 and 0.9 g/cm^3 bulk densities are presented in Figure 22. Unlike the pullout behavior, the lateral behavior of screws does not change notably with changing the aerated slurry bulk density. Figure 23 presents typical screw lateral behavior in aerated slurry-infiltrated chicken mesh sheets with 4, 8 and 12 layers of chicken mesh.

The increase in the number of chicken mesh layers is observed to significantly benefit the lateral load-carrying capacity and the ductility of the screw lateral behavior. Closer observation of failure modes under lateral loading (Figure 24) indicated that the lateral behavior of screws (and also nails) in aerated slurry-infiltrated chicken mesh is largely a result of the interactions of screws with the chicken mesh reinforcement. This observation explains the significant effects of the number of chicken mesh layers on the screw lateral behavior. At extreme levels of bulk density, the screw or nail lateral behavior could be affected by the bulk density of the aerated slurry. This is because the tensile behavior of chicken mesh within aerated slurry-infiltrated chicken mesh depends upon the restraining effect of the aerated slurry matrix which is a function of the modulus and strength of the aerated slurry.

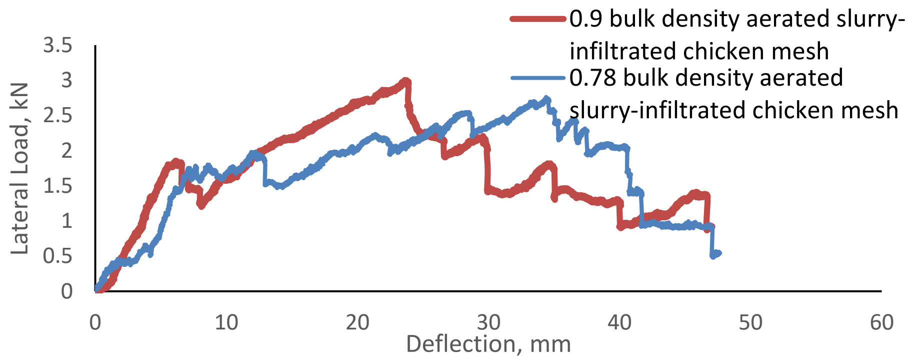

Figure 22. Typical lateral load-deflection behavior of exterior screw in aerated slurry-infiltrated chicken mesh sheets of different bulk densities.

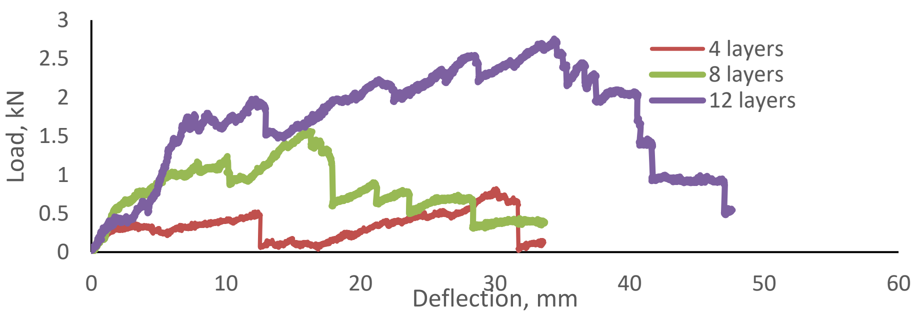

Figure 23. Lateral load-deflection behavior of exterior screw in aerated slurry-infiltrated chicken mesh sheets with different numbers of chicken mesh layers.

Figure 24. Visual appearance of aerated slurry-infiltrated chicken mesh sheets after failure under lateral loading of a screw.

3.3.3 Screws and Nail Cyclic Lateral Behavior in Aerated Slurry-Infiltrated Chicken Mesh Sheets

Figure 25 presents typical cyclic load-displacement curves obtained with two-common nail of 101.6 mm length and 4.19 mm diameter applied to aerated slurry-infiltrated chicken mesh sheets. The sheets and the nails after application of cyclic tests are shown in Figure 26. The nails essentially cut into the aerated slurry, but had to drag the layers of chicken mesh in the process (with nails themselves experiencing some plastic deformations in the process). This behavior led to a pinched but stable hysteretic behavior. At each displacement level, the load could be largely restored under repeated displacement cycles. In the case with nails aligned parallel to the load direction (Figure 25a), that is not very relevant to the indigenous building system considered here, the hysteretic energy dissipation at each displacement level occurred in the first cycle, with minimal energy dissipation occurring in subsequent cycles of the same displacement. Increased displacement levels, however, restored the energy dissipation capacity of nails during the first cycle. The peak load continued to increase with increasing deformation (within the range considered here), which is due to the resistance provided by the chicken mesh layers that are dragged with the nail. With nails perpendicular to the load direction (Figure 25b), the peak load as well as the hysteretic energy dissipation are more favorable. Peak loads approach twice those obtained with nails aligned parallel to the load direction. As far as the hysteretic energy dissipation capacity is concerned, subsequent cycles at constant displacement provide reduced (compared to the first cycle) but still notable energy dissipation capacity (that is unlike the case with nails aligned parallel to the load direction). The peak load continues to increase with increasing displacement, but at a faster pace than that observed with nails aligned parallel to the load direction.

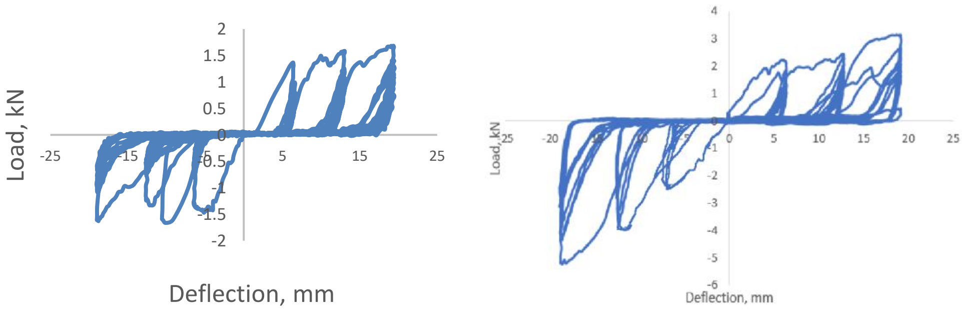

(a) Nails aligned parallel to load (b) Nails aligned perpendicular to load

Figure 25. Typical load-displacement curves in cyclic lateral loading of nails with different configurations applied to aerated slurry-infiltrated chicken mesh sheets.

(a) (b) (c)

Figure 26. Typical appearances of sheets and nails after performance of cyclic lateral tests: (a) sheet with nails aligned parallel to the loading direction; (b) sheet with nails aligned perpendicular to the loading direction; and (c) nails.

Figure 27a presents typical cyclic lateral load-displacement curves obtained with the single exterior screw of 101.6 mm length and 4.19 mm diameter applied to an aerated slurry-infiltrated chicken mesh sheet. Figure 27b presents typical cyclic load-deflection curves for a single common nail of 101.6 mm length and 4.19 mm diameter tested similar to the screw. The peak load continues to increase with increasing displacement within the displacement range considered here. The values of load at similar deflections were comparable for the nail and the screw which had similar lengths and diameters.

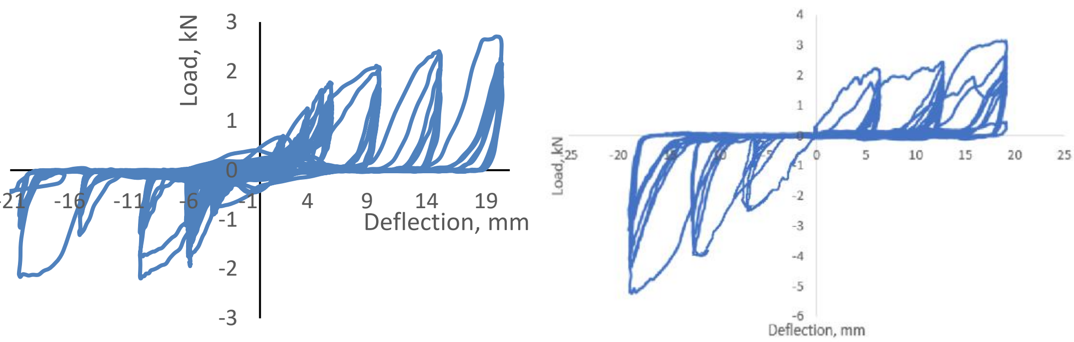

(a) Specimen with screw (b) Specimen with common nail

Figure 27. Typical load-displacement curve obtains from cyclic connection test, (a) exterior screw with 101.6 mm length and 4.19 mm diameter, (b) common nail with 101.6 mm length and 4.19 mm diameter

CHAPTER 4
BEHAVIOR OF A LIGHTWEIGHT FRAME MADE WITH AERATED SLURRY-INFILTRATED CHICKEN MESH UNDER CYCLIC LATERAL LOADING

4.1. Introduction

Aerated concrete is traditionally viewed as an insulating (non-structural) building material. A primary premise of the work reported herein is that a reinforcement system with high specific surface area would enable use of aerated concrete in structural applications. The high specific surface area and the confining role of such reinforcement was hypothesized to benefit the structural performance of aerated concrete. Construction with reinforcement systems of high specific surface area would be challenged by the congestion of reinforcement which is not favorable to convenient placement and consolidation of aerated concrete. An aerated slurry of high flowability was used in this work to thoroughly penetrate the congested reinforcement system, facilitating thorough consolidation and desired interfacial interactions with the reinforcement. This work chose chicken mesh (hexagonal 20-gauge galvanized poultry netting) as a steel reinforcement system of high specific surface area due to its broad availability across the world.

Concrete structures generally rely on frames as the primary lateral load-resisting structural systems (Arroyo and Gutiérrez 2016, Abd-Elhamed and Mahmoud 2017, Ruiz-García and Aguilar 2017). Reinforced concrete frames can be designed to provide high levels of ductility and (hysteretic) energy dissipation capacity for efficient resistance of seismic forces. Aerated slurry-infiltrated chicken mesh can, due to the high specific surface area of steel reinforcement, provide distinctly high levels of ductility and energy dissipation capacity. The work reported herein evaluated the structural performance of an aerated slurry-infiltrated chicken mesh from under cyclic lateral loads (He, Lam et al. 1998, Rose 1998). The data generated on the ductility, hysteretic energy absorption capacity and the lateral load-bearing capacity of the frame, accompanied with structural analyses of the frame, provide insight into the merits of aerated slurry-infiltrated chicken mesh as a robust building material for construction of seismic-resistant building systems.

4.2. Materials and Methods

4.2.1. Aerated Slurry

Aeration introduces a homogenous system of fine air bubbles into the cement paste. This is accomplished using foaming agents that stabilize the air voids generated via agitation of the mixing water of slurry that incorporates the foaming agent (Nambiar and Ramamurthy 2007, Ramamurthy, Nambiar et al. 2009, Zhang, Provis et al. 2014). Preparation of the aerated slurry started with production of foamed water. For this purpose, a foaming agent extracted from plants (saponin) blended with the mixing water at 1200 rpm rotational speed, using a mixing blade attached to a drill (Figure 28). The foamed mixing water was then added to cement at water/cement ratio of 0.5. Mixing was accomplished in a mortar mixer for 2 minutes.

Figure 28. Preparation of foamed water.

The aerated slurry used to infiltrate the chicken mesh (Figure 3b) comprised cement: water: saponin at 1: 0.5: 0.0006 weight ratios, with a bulk density in hardened state of 0.9 g/cm^3. Cube specimens of plain aerated slurry with 50 mm dimensions were also prepared for performance of compression tests. The molded specimens were stored in sealed condition (>95% relative humidity) at room temperature) for 7 days, and then subjected to compression testing. The average compressive strength was measured at 5 MPa.

4.2.2. Chicken Mesh

The chicken mesh considered in this experimental program (Figure 29) comprised wire gauge No. 20 (with 0.88 mm diameter, 0.608 mm^2 cross sectional areas) configured hexagonally with wire spacing of 25 mm. Chicken meshes are available with different wire diameter and spacing. Commonly available chicken meshes are made with wires of different diameters; the spacing of hexagonally configured wires are generally increased with increasing wire diameter in order to provide comparable wire cross-sectional areas per unit width. Given the relatively large layers of chicken mesh that need to be infiltrated with aerated slurry, the preference in this investigation was for chicken meshes with larger wire diameter and spacing. Figure 30 depicts the anisotropic structure of chicken mesh, which provides higher strength in the longitudinal direction and lower strength in the transverse direction.

Figure 29. The chicken mesh used in this experimental program.

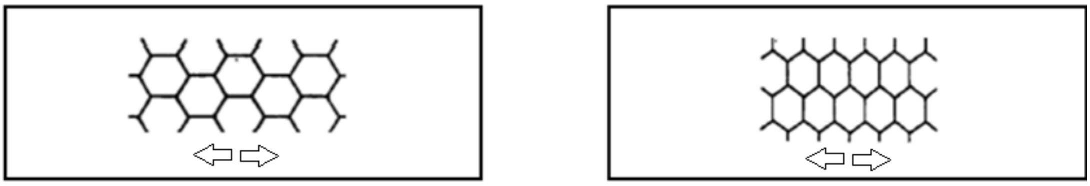

Figure 30. Chicken mesh orientations: longitudinal (left), and transverse (right).

4.2.3. Aerated Slurry-Infiltrated Chicken Mesh

Given the fine diameter of the chicken mesh wires, a relatively low volume fraction (e.g., 1%) of chicken mesh produces a relatively congested reinforcement system. As a result, cementitious materials with normal fresh mix rheology cannot be used in this application. The need to infiltrate multiple layers of chicken mesh led to the selection of a flowable slurry as the binder for use with chicken mesh reinforcement. Aerated slurry was used in this application to lower the density of structural materials for ease of installation and reduction of seismic forces. Aerated concrete is usually used as insulation and not in structural applications. It was hypothesized that the high specific surface area and the confining action of chicken mesh would enhance the mechanical performance of the resultant aerated slurry infiltrated chicken mesh to suit structural applications.

In chicken mesh, wires are oriented in different directions. Chicken mesh thus offers a high level of flexibility when subjected to tension, which is due to a tendency towards alignment of wires along the direction of tensile force. Their low stiffness excludes chicken mesh from structural applications. When placed within a matrix (aerated slurry in this case), however, the wires in chicken mesh are restrained against realignment by the matrix. Depending on the extent of this restraint, the tensile force-resisting capacity of wires would be mobilized from the beginning. This raises the stiffness of chicken mesh, which could translate aerated slurry infiltrated chicken mesh into a structural building material. Semi-empirical equations were developed to express the tensile and compressive strengths of aerated slurry infiltrated chicken mesh, as described below.

4.2.4. <u>Aerated Slurry Infiltrated Chicken Mesh Frame</u>

The models presented earlier predicting the flexural strength of aerated slurry infiltrated chicken mesh were verified using the experimental results.

The tensile strength of aerated slurry infiltrated chicken mesh (σ_T) was expressed as follows:

$$\sigma_T = \alpha \rho f_y$$

where, ρ = area fraction of the chicken mesh wires (irrespective of their orientation) at a cross-section that is perpendicular to the tensile stress direction; f_y = yield stress of the chicken mesh wires (310 MPa); and α = an empirical efficiency factor which reflects the degree of restraint provided by the aerated slurry against realignment of wires (0.56 based on experimental results).

In compression, the composite behavior of aerated slurry infiltrated chicken mesh produces a compressive strength that can be expressed as follows:

$$\sigma_C = \beta\rho f_y + \gamma f_c'$$

where, σ_c = compressive strength; β = efficiency factor of chicken mesh reinforcement in compressive (it was assumed to be similar to the efficiency factor of chicken mesh in tension, that is 0.56); and γ = efficiency factor of aerated sully in compression, which was surprisingly found (in compression tests performed on an aerated slurry infiltrated chicken mesh) to be quite large (close to 5).

Using concepts similar to those used with reinforced concrete, the nominal flexural strength (M_n) of an aerated slurry-infiltrated chicken mesh cross-section (Figure 31) can be expressed as follows:

$$M_n = \alpha\rho f_y b(h - a)(\frac{h}{2})$$

where, 'a' was assumed to be equal to the depth of neutral axis c, considering the highly ductile behavior of aerated slurry infiltrated chicken mesh. A constant compressive stress was assumed up to depth 'a' in order to simulate the nonlinear compressive stress distribution. The value of 'a' can be derived based on the equilibrium of tensile and compressive forces generated at the section subjected to bending moment:

$$\alpha\rho f_y(h - a) = \left(\beta\rho f_y + \gamma f_c'\right)a$$

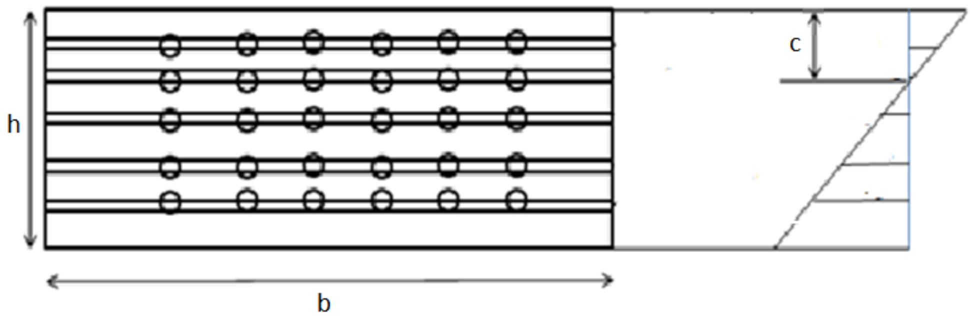

Figure 31. Cross-section and flexural strain distribution of aerated slurry infiltrated chicken mesh.

An aerated slurry infiltrated chicken mesh frame with 1.75 m height and 1.4 m width was designed to withstand a concentrated in-plane load of 8 KN applied at its top. The maximum bending moment under this loading condition is: M= F_t.h /2 = 7,000 N.m. The cross-section designed to resist this bending moment had 10 cm width and 25 cm height, reinforced with 30 layers of chicken mesh (with the chicken mesh layers oriented longitudinally along the element axis). The area fraction of longitudinally oriented chicken mesh layers at cross-sections is 1.5%. The resultant tensile and compressive strengths of the aerated slurry-infiltrated chicken mesh would be:

$\sigma_T = \alpha\rho f_y = 0.56x0.016x310 = 2.75\ MPa$

$\sigma_C = \beta\rho f_y + \gamma f_c'$ = 0.56x0.016x310 + 5x2.5 = 15.2776 MPa

Equilibrium of tensile and compressive forces can be used to calculate the value of 'a' (assumed to be equal to the depth of neutral axis "c" in Figure 4) required for calculating the nominal flexural strength:

$\sigma_C.a = \ \sigma_T.(h-a)$

15.2776xa = 2.75x (250-a)

a = 38.29 mm

The flexural strength of the aerated slurry infiltrated chicken mesh can now be calculated as:

$M_n = \alpha\rho f_y b(h-a)(\frac{h}{2})$ = 0.56x0.016x310x100x(250-38.29)x(250/2) = 7376.50 N.m

The nominal bending moment flexural strength of 7,376.5 N.m exceeds the required flexural strength of 7,000 N.m by 5%.

Figure 32a shows the formwork with chicken mesh reinforcement placed in it. The slurry was simply poured onto the chicken mesh (Figure 32b) to infiltrate the preplaced chicken mesh layers. After pouring of slurry, the frame was covered with plastic sheet to mitigate moisture loss. This allowed for curing at >95% relative humidity, that was achieved using the vapor released from the slurry during curing. The frame was cured at ambient temperature for 14 days.

(a) Formwork with preplaced chicken mesh (b) Infiltration of Chicken mesh

Figure 32. Construction of the aerated slurry-infiltrated chicken mesh frame.

4.2.5. Cyclic Testing

The frame behavior was evaluated under quasi-static cyclic lateral loading. The test procedure involved application of reversed load cycles of progressively increasing lateral displacements until the first major event (FME), defined here as yielding, occurred. Three reversed cycles of progressively increasing displacement amplitude were applied before the FME was reached. Subsequent loading followed the Sequential Phase Displacement (SPD) procedure which involves application of degradation and stabilization cycles at a constant displacement amplitude before progressing to the next phase with a greater displacement. The first cycle in a phase is applied with a larger displacement, and is proceeded by three degradation cycles; subsequent application of three stabilization cycles completes the phase. Stabilized response is achieved when the decrease in resistance between two successive stabilization cycles is less than 5% (Soudki, West et al. 1996). If the decrease in resistance is more than 5%, additional stabilization cycles should be conducted. The frame tested in this study stabilized in five cycles. The procedure then moves on to the next phase (Salenikovich, Dolan et al. 1999, Gatto and Uang 2003, Ibarra, Medina et al. 2005).

Cyclic testing of the frame was performed in accordance with ASTM E2126 Method A, that closely follows the SPD procedure developed by TCCMAR (Porter 1987) with few modifications. The SPD procedure is based solely on the First Major Event (FME), where FME is defined as the displacement at which the structure starts to deform inelastically (anticipated yield displacement) (Krawinkler 2009). ASTM E2126, on the other hand, takes into account both FME and ductility ratio when determining the initial amplitude of each phase in the test protocol. In general, the SPD protocol is displacement-controlled, and involves triangular reversed cycles at increasing displacement levels. The displacement increase in ASTM E2126 is based on FME and ductility ratio. The SPD procedure begins with at least three incremental levels of three cycles each, within the elastic displacement region up to the First Major Event (FME). The SPD method recommends 200% of the FME as the displacement increment for each phase in the case of ductile systems (Salenikovich, Dolan et al. 1999, Gatto and Uang 2003).

The test protocol devised here, based on ASTM E2126 requirement, comprised 15 steps of displacement increase, with trailing cycles after each peak cycle as shown in Table 7.

Table 7. Test protocol for evaluation of the frame performance under cyclic lateral loads

Load step	Drift	Peak Displacement, cm	Trailing Cycle Displ.	# of trailing cycles
1	0.050%	0.048	0.048	5
2	0.075%	0.072	0.054	6
3	0.100%	0.096	0.072	6
4	0.20%	0.192	0.144	3
5	0.3%	0.288	0.216	3
6	0.4%	0.384	0.288	3
7	0.7%	0.672	0.504	2
8	1.00%	0.960	0.720	2
9	1.50%	1.440	1.080	2
10	2.00%	1.920	1.440	2
11	2.50%	2.400	1.800	2
12	3.00%	2.880	2.160	2
13	4.00%	3.840	2.880	2
14	4.50%	4.320	3.240	2
15	5.00%	4.800	3.600	2

The column bases were fixed in an aerated slurry-infiltrated chicken mesh footing, and installed on a reaction frame (Figure 33) for in-plane lateral cyclic loading per ASTM E564. A load cell and a displacement transducer were used to collect the load and displacement data, using a data acquisition system, under cyclic lateral loads.

Figure 33. The test setup used for performance of cyclic tests on the aerated slurry-infiltrated chicken mesh frame.

4.3. Test Results and Discussion

The frame failed by plastic hinge formation in beam, as expected from the strong column-weak beam approach adopted for seismic design of the frame. Figure 34 shows the plastic hinge formation in beam near the beam-column joint under repeated load cycles. The top part of the plastic hinge exhibited multiple cracking, while one crack formed at the bottom, which widened and connected to top cracks under cyclic deformations of growing amplitudes.

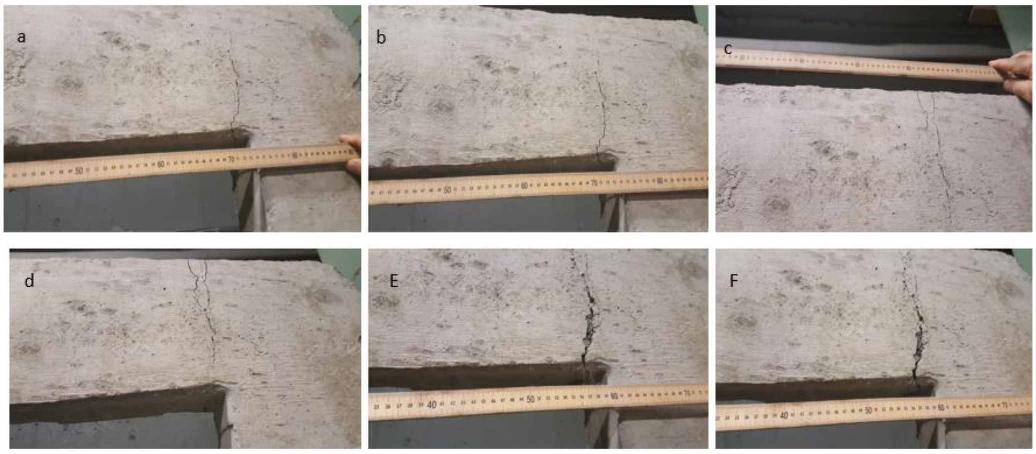

Figure 34. Plastic hinge formation in beam near the beam-column joint under reversed cycling testing with growing displacement amplitudes.

The cyclic load-deflection curve produced for the frame is presented in Figure 35 together with the initial envelope (connecting the initial peak loads at the initial load achieved for each displacement) as well as the stabilized envelope (connecting the stabilized peak loads after repeated cycles at each deformation) (Dolan and Heine 1997). The displacement cycles were unsymmetrical in this test due to the size constraints of the reaction frame used in this test. Figures 36a and 36b shows the average initial and stabilized envelopes, respectively, obtained by averaging the corresponding envelope curves produced in opposite displacement directions (Dolan and Johnson 1996, Dolan and Heine 1997).

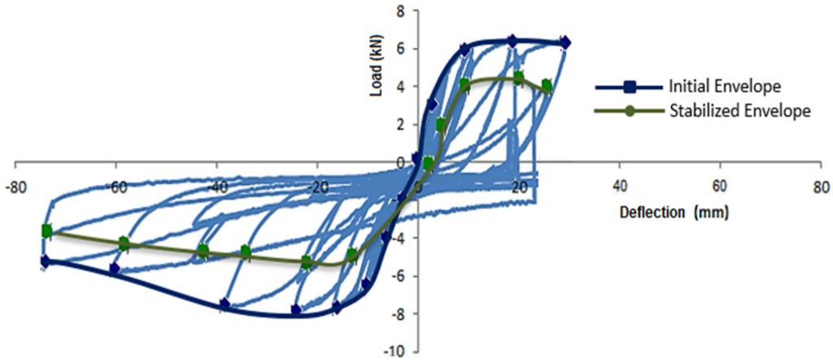

Figure 35. The hysteretic response, and the initial and stabilized envelopes of the frame subjected to cyclic loading per SPD (ASTM E2126) test method.

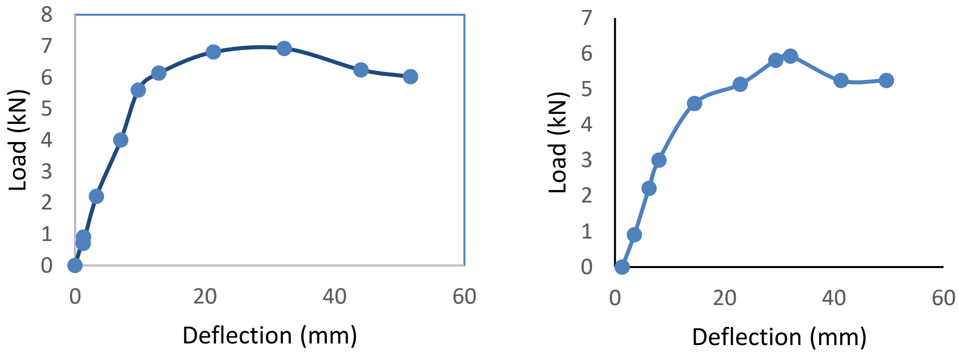

(a) Initial envelope

(b) Stabilized envelope

Figure 36. Averaged initial and stabilized envelope curves of the aerated slurry-infiltrated chicken mesh frame.

A comparative study was made of the behavior of the aerated slurry-infiltrated chicken mesh frame versus lateral load-carrying system of similar geometric attributes comprising either oriented strandboard (OSB) or hardwood subjected to comparable cyclic lateral loads (Toothman 2003). Figure 37 shows the average initial envelopes of these systems. The aerated slurry-infiltrated chicken mesh frame is observed to provide ductility levels comparable to those of lateral load-carrying systems based on OSB and hardwood. The peak load-carrying capacity of the frame is more than those of systems based on OSB and hardwood; such comparisons, however, should also account for the weight of different systems.

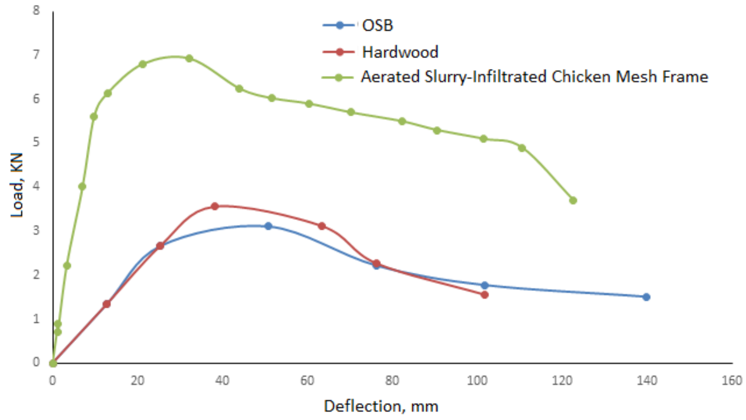

Figure 37. Averaged initial envelope curves of the aerated slurry-infiltrated chicken mesh frame versus those of lateral load-carrying systems based on OSB and hardwood.

The envelope curves introduced above can be used, following the ASTM E2126 procedures, to derive the Equivalent Energy Elastic Plastic (EEEP) curve that represents an elasto-plastic interpretation of the aerated slurry-infiltrated chicken mesh behavior. The EEEP curve (Figure 11) encompasses the same order of magnitude area as the actual load-displacement curve (form the origin to the ultimate displacement). This area is a measure of the toughness of the system. Toughness is defined here as the energy required to fail the structural system. The EEP curve shown in Figure 38 incorporates a yield force(P_{yield}) and the corresponding displacement (Δ_{yield}), the failure displacement (Δ_u), the area under the load-displacement curve, and the elastic stiffness of the structural system.

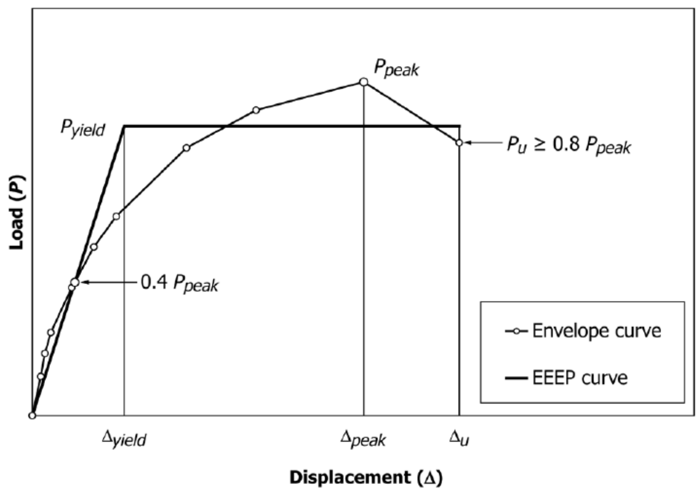

Figure 38. Definition of the EEEP curve (ASTM E2126).

Figure 39 shows the averaged initial and stabilized envelope curves of the slurry-infiltrated chicken mesh frame, and also the EEEP curve corresponding to the initial envelope curve. Elastic stiffness, k_e, can be determined as the slope of the secant passing through the origin and the point on the load-displacement curve (or envelope curve) that is equal to 40% of the peak load, F_{peak}. The slope of this line is used to locate the elastic portion of the EEEP curve. In addition, it is used to find other parameters such as the yield load, yield displacement, and the ductility ratio.(Kesner, Billington et al. 2003)

$$\textit{Elastic Stiffness} = k_e = \frac{0.4F_{Peak}}{\Delta_{0.4Fpeak}}$$

Elastic stiffness is a good indicator of the stiffness that a frame would exhibit when subjected to low to moderate displacements (Salenikovich 2000). The elastic stiffness obtained using the initial envelope curve for the aerated slurry-infiltrated chicken mesh following the above procedure is shown in Figure 40, and compared with later load resisting systems of comparable geometry made with OSB or hardwood sheeting. The elastic stiffness of the aerated slurry-infiltrated chicken mesh is observed to be higher than those provided by alternative lateral load resisting systems

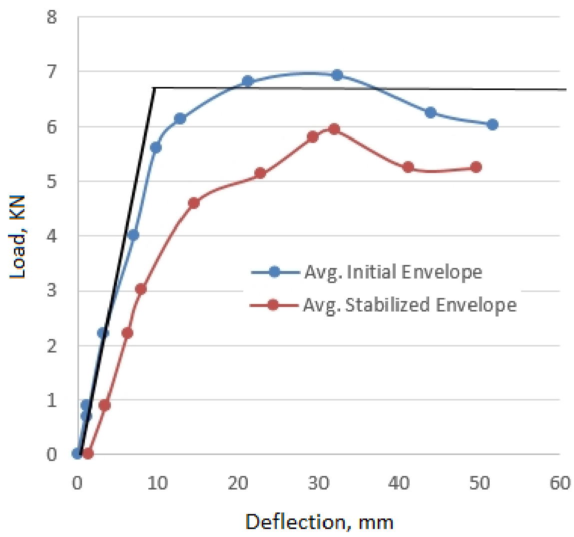

Figure 39. The initial and stabilized envelope curves of the aerated slurry-infiltrated chicken mesh frame, and the EEEP curve corresponding to the initial envelope.

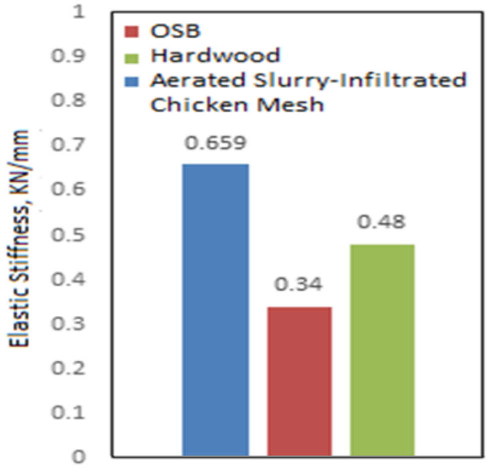

Figure 40. Elastic stiffness of different sheathing materials

Following the ASTM E2126 procedures, failure load was calculated as 80% of the peak load. Displacement at failure is another key parameter in assessing the seismic resistance of a lateral load-carrying system. The ability of a structure to dissipate energy arises partly from its ability to deform without failing (Park 1989, Salonikios, Kappos et al. 2000). Table 8 compares the failure load and the displacement at failure of the aerated slurry-infiltrated chicken mesh frame versus alternative lateral load-resisting systems with comparable geometry which are made with oriented strandboard (OSB) and hardwood sheathing. The aerated slurry-infiltrated chicken mesh frame is observed to provide a relatively high failure load but lower displacement at failure when compared with the alternative systems. A review of the initial envelopes of these systems, however, indicates that the overall ductility of the three systems is comparable, and the relatively low displacement at failure of the aerated slurry-infiltrated chicken mesh frame is a result of the approach taken by ASMT E2126 to define this displacement.

Table 8. Failure load and displacement at failure of aerated slurry-infiltrated chicken mesh frame versus alternative lateral load-carrying systems of comparable geometric attributes.

Lateral Load-Carrying System	Failure Load, kN	Displacement at Failure, mm
Aerated slurry w/chicken mesh	5.54	32.26
OSB	3.11	83
Hardboard	3.29	76

4.3.1. Yield load and yield displacement

Yield load is determined based on an approximation of the first major event, which is the theoretical load and displacement at which the structure starts to deform inelastically . For the area under the load-displacement curve and the EEEP curve to be equal, the value of F_{yield} is found where the area of the load-displacement curve equals the area of the EEEP curve . The area under the load-displacement curve (A) can be computed by integrating the initial envelope curve between x=0 to x=32.6 mm (the failure displacement as presented in Table 9). The value of F_{yield} can then be calculated as follows:

$$F_{yield} = \frac{-\Delta_u \pm \sqrt{\Delta_u^2 - \frac{2A}{k_e}}}{\frac{-1}{k_e}}$$

Where F_{yield}= Yield Load (Kip, KN), A = the area (kip.in, KN.mm) under the load-displacement curve from the origin to the failure displacement ($\Delta_{failure}$), and k_e = elastic Stiffness (kip/in, kN/mm). Once F_{yield} is determined, the yield displacement can be calculated using the following relationship:

$$\text{Yield Displacement } (\Delta_{yield}) = \frac{F_{yield}}{k_e}$$

Table 9. The parameters required for calculation of the yield load (and the calculated value of yield load).

Parameter	Numerical value
A, mm^2	255.2
Ke, KN/mm	0.659
$\Delta_{failure}$, mm	8.26
F_{yield}, KN	5.445

4.3.2. Ductility

Ductility is an important characteristic of a structural system, which reflects its ability to yield and deform inelastically without failure. The ability of structural member to bend but not fail is important exposure to sudden and powerful cycles of an intense earthquake. Different measures have been used to express the ductility of a structure. The most commonly accepted definition is that of ASTM E2126, which defines the ductility factor, μ, as the ratio of the failure displacement to the yield displacement. The ductility ratio, derived from test results, is defined as the displacement at failure load divided by the displacement at yield load (Salenikovich, Dolan et al. 1999, Thomsen IV and Wallace 2004)

$$\text{Ductility Ratio} = \mu = \frac{\Delta_{failure}}{\Delta_{yield}}$$

This value represents the relative displacement that a structure can undergo from yielding until failure. It reflects the ability of ductile structural systems to undergo further displacements beyond Δ_{peak}. When the structural component has reached its capacity, it transfers additional load onto other components. The ductility factor introduced above is the ratio of two displacements. If a structure undergoes large deformations before failure but has a large yield displacement, the structure is not necessarily a ductile system. The reverse is also true, so ductility should always be considered together with other performance indicators. Although ductility is an important characteristic, it should be noted that it is not a material property and caution should be used when comparing different structural systems. Given the variations that exists when calculating the elastic stiffness and yield load, a large margin for error and inconsistent results may be encountered.

The ductility factor of structural systems comprising sheathing materials varies from 4 to 10 for both OSB and hardboard (Toothman 2003) , compared to a ductility factor of 10.9 calculated for the aerated slurry infiltrated chicken mesh frame using Equation (8). The higher elastic stiffness of the frame tends to reduce its yield displacement, which raises the calculated value of ductility. These results point at the ductile behavior of the aerated slurry-infiltrated chicken mesh frame, and its ability to yield and undergo inelastic deformation to dissipate the input energy of severe earthquake ground motions.

CHAPTER 5

STRUCTURAL EVALUATION OF A LIGHTWEIGHT BUILDING SYSTEM MADE WITH LOCALLY AVAILABLE MATERIALS

5.1. Introduction

Aerated concrete with bulk densities less than 1 g/cm^3 is generally viewed as a non-structural material that offers thermal insulation qualities(Narayanan and Ramamurthy 2000, Abdullah, Hussin et al. 2006, Memon, Sumadi et al. 2006). The work reported herein employed chicken mesh (poultry netting) to enhance the structural qualities of aerated concrete for load-bearing applications. Chicken mesh, when used at 2-4 vol.% in aerated concrete, produces a composite material with significantly enhanced mechanical properties that result from the synergistic actions of chicken mesh and aerated concrete in the context of the composite materials. The term aerated concrete is altered to aerated slurry in this application because a highly flowable aerated concrete would be needed to infiltrate the closely spaced wires of chicken mesh used at the required volume fraction. The composite material is thus referred to as 'aerated slurry-infiltrated chicken mesh'. In this composite, the high specific surface area of chicken mesh and the close spacing of its wires significantly enhance the compressive strength and the dimensional stability of the aerated slurry. The restraining effects of the aerated slurry against reorientation of the chicken mesh wires, on the other hand, enables mobilization of the tensile load-carrying capacity of the chicken mesh wires at structurally viable deformations. These synergistic effects produce a lightweight composite material with a desired balance of compressive and tensile strengths, ductility and toughness. The combination of aeration of matrix and use of chicken mesh at 2-4 vol.% enables application of screw (and nail) for joining of aerated slurry-infiltrated chicken mesh components. The interactions of screws with the aerated slurry and the layers of chicken mesh reinforcement provides for highly ductile behavior when screws are subjected to pullout and lateral loads.

Ferrocement is the building system with attributes similar to aerated slurry-infiltrated chicken mesh. (Aboul-Anen, El-Shafey et al. 2009, Ahmad, Arif et al. 2014)The matrix in ferrocement is commonly a conventional (normal-weight) mortar of relatively low flowability, which is troweled into layers of mesh that are generally coarser than chicken mesh(Naaman 2000, Sreevidya, Anuradha et al. 2012), with smaller specific surface area and greater spacing of wires (rods). Minor work has been performed on ferrocement with chicken mesh reinforcement (Naaman 2000, Wafa and Fukuzawa 2010).

An experimental investigation was conducted in order to comprehend the structural performance of aerated slurry-infiltrated chicken mesh building elements and subcomponents(Desayi and Reddy 1991, Krawinkler 2009, Heinzmann, Etter et al. 2012). Structural analysis techniques were developed for this building system, and a building structure was designed with aerated slurry-infiltrated chicken mesh.

5.2 Experimental Program

5.2.1 Introduction

Structural elements and subcomponents made with aerated slurry-infiltrated chicken mesh were evaluated under different force systems. The elements evaluated here included sheets, beams and columns. The subcomponents tested in this experimental program included frames with sheets screwed to it, which were subjected to cyclic lateral loading (representing seismic effects).

5.2.2 A Brief Review of the Material Properties of Aerated Slurry-infiltrated Chicken Mesh

Aerated slurry-infiltrated chicken mesh is produced by preparing a highly flowable aerated slurry of 0.6 water/cement ratio and bulk density of less than 1 g/cm^3. This investigation was performed with aerated slurries of 0.75 and 0.9 g/cm^3 bulk density. Structural elements are produced by preplacing the required chicken mesh layers in the formwork, followed by infiltration of the chicken mesh layers with aerated slurry. Figure 41 shown a chicken mesh, and Figure 42 depicts the process of infiltrating the chicken mesh layers placed in a form with aerated slurry. Chicken mesh is used in this application at 2-4% volume fraction. The anisotropic nature of chicken mesh requires their orientation so that the strongest direction is aligned with the direction of largest tensile stresses.

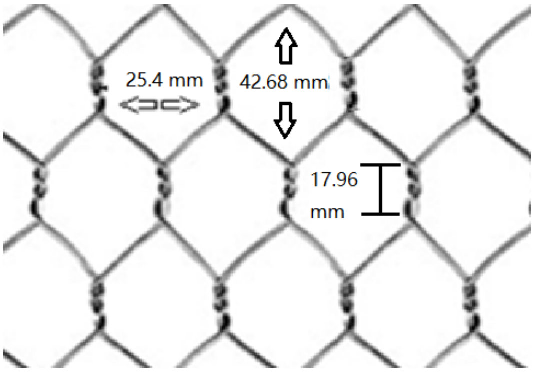

Figure 41. An example of chicken mesh.

Figure 42. Infiltration of the chicken mesh layers placed in a form with aerated slurry.

The tensile strengths provided by aerated slurry-infiltrated chicken mesh range from 1.6 to 5 MPa, their flexural strengths from 3 to 8 MPa, and compressive strength from 15 to 20 MPa. Figure 43 shows a typical tensile stress-strain relationship of aerated slurry-infiltrated chicken mesh. The ductile behavior observed here in tension is also noted under flexural and compressive load systems.

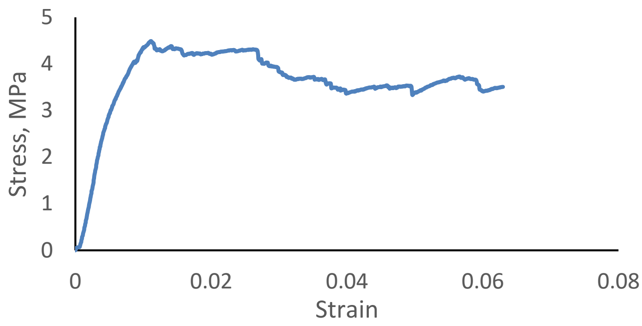

Figure 43. Typical tensile stress-strain behavior of aerated slurry-infiltrated chicken mesh.

5.2.3 Aerated Slurry-Infiltrated Chicken Mesh Sheets

The aerated slurry used for preparation of sheets comprised cement: water: saponin (foaming agent) at 1: 0.6: 0.00045 weight ratios. Aerated slurry-infiltrated chicken mesh sheets were subjected to flexure and punching shear tests. The chicken mesh used in this investigation was made with wires of 0.88 mm diameter and 310 MPa yield strength. Sheets of different thickness and number of chicken mesh layers were tested in Flexure (Table 10). The chicken mesh layers were aligned so that their stronger (longitudinal) direction was oriented with the direction of the tensile stress generated under flexural loading. The sheets subjected to flexural loading had length and width of 1219 and 609 mm, respectively. They were subjected to three-point loading over a span of 1,000 mm. The flexure test setup is shown in Figure 44. Flexural loading was applied quasi-statically following the general procedures of ASTM D790.

Figure 44. The setup used for flexure testing of aerated slurry-infiltrated chicken mesh sheets.

Table 10. The thickness, number of chicken mesh layers, and the volume fraction and cross-section area fraction of chicken mesh reinforcement.

Specimen No.	Thickness, mm	Chicken Mesh Reinforcement		
		No. of Layers	Volume Fraction, %	Area Fraction, %
1	25.40	12	3.63	3.04
2	31.75	16	3.87	3.24
3	38.10	18	3.63	3.04
4	50.80	24	3.63	3.04

The aerated slurry-infiltrated chicken mesh sheets subjected to punching shear tests were 609 mm by 609 mm planar dimensions with the following thickness and reinforcement conditions: (i) 25.4 mm thickness and 12 layers of chicken mesh (3.6% chicken mesh volume fraction); and (ii) 31.75 mm thickness and 16 layers of chicken mesh (3.8% chicken mesh volume fraction). The punching shear test setup is shown in Figure 45. The specimen was loaded on a 5 cm diameter area, with the four corners of the specimen fixed (Guandalini, Burdet et al. 2009, Heinzmann, Etter et al. 2012). The values of load and deflection were recorded during the tests.

Figure 45. Punching shear test setup

5.2.4 Aerated Slurry-Infiltrated Chicken Mesh Beams

Three similar aerated slurry-infiltrated chicken mesh beams were tested under lateral loading, with load configurations selected to encourage flexural failure in two beams, and shear failure in the third one. The width and height of the beam cross sections were 102 mm and 229 mm, respectively. The total beam lengths were 1,006 mm and 520 mm, respectively. The test spans of the beams were 900 and 500 mm in flexure and shear tests, respectively. The chicken mesh reinforcement in beams comprised 30 layers of mesh places in folded form, and e layers of mesh wrapped around them. The total number of chicken mesh layers was thus 38 layers distributed rather uniformly around the full height. The strong direction of chicken mesh was oriented along the length of the beam specimens. The flexure and shear test setups are shown in Figures 46, respectively. Flexure tests were performed under three-point loading. In shear tests, two loads were applied at 100 mm distance from each support. Loads were applied quasi-statically using a servovalve-controlled hydraulic cement system up to failure (Aboul-Anen, El-Shafey et al. 2009). Loads and deflections were monitored throughout tests using load cells, deflection transducers and a high-speed data acquisition system.

(a)

(b)

Figure 46. (a)Flexure test setup, (b) Shear test setup.

5.2.5 Aerated Slurry-Infiltrated Chicken Mesh Columns

Prismatic aerated slurry-infiltrated chicken mesh column specimens were tested in compression. The column specimens were 102 mm by 102 mm in cross-section, with a total height of 229 mm. The chicken mesh reinforcement in columns were similar to those in beams described earlier. A side view of the column specimen is schematically depicted in Figure 47.

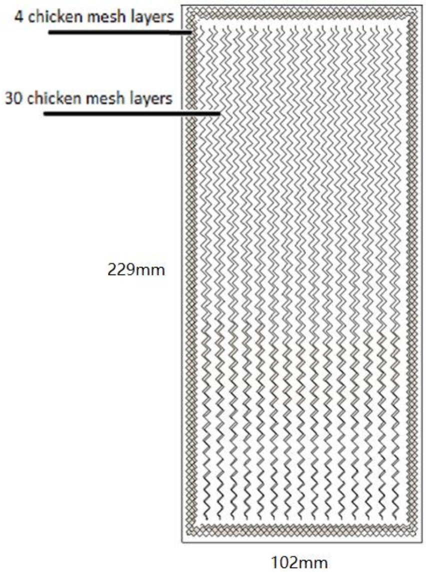

Figure 47. A schematic depiction of the side view of the aerated slurry-infiltrated chicken mesh column test specimen.

5.2.6 Aerated Slurry-Infiltrated Chicken Mesh Subcomponents

The subcomponent test specimens comprised aerated slurry-infiltrated chicken mesh frames to which aerated slurry-infiltrated chicken mesh sheets were nailed. Two categories of subcomponents were tested. One (Figure 48) comprised one frame with two sheets nailed to both its sides. The other category (Figure 50) comprised two frames with interior and exterior (wall, ceiling and roof) sheets nailed to it. The subcomponent with one frame was subjected to cyclic lateral loading in the plane of the frame (Figure 49). A frame (without sheets nailed to it) was also tested for comparison purposes. The subcomponent with two frames was subjected to cyclic lateral loading out of the plane of the frames (Figure 50). The lateral loads in both cases were applied at the beam level, with the columns bases spaced in rigid footings that were fixed to the test frame.

The aerated slurry-infiltrated chicken mesh sheets used in these tests were 25.4 mm thick with 12 layers of chicken mesh reinforcement. The frames comprised beams and columns with 102 width and 254 mm height. The height and width of the frames were 1.75 and 1.4 m, respectively. The nails used here had a diameter of 4.12 mm, and a length of 101.6 mm, the nails were applied at a spacing of 26 cm.

Figure 48. The subcomponent comprising one frame with two sheets nailed to it.

Figure 49. Test setup for cyclic in-plane lateral loading of the subcomponent with one frame.

Figure 50. Test setup for cyclic lateral loading of the subcomponent comprising two frames with sheets nailed to their interior and exterior, and loading applied perpendicular to the frame planes.

A servovalve-controlled hydraulic actuator was used to apply quasi-static cyclic lateral loads to the building subcomponents per ASTM E564. Loads and deflections were monitored throughout the tests using a load cell and a displacement transducer with a high-speed data acquisition system. The test procedure involved application of reversed load cycles of progressively increasing lateral displacements until the occurrence of the first major event (FME), defined here as yielding. Three reversed cycles of progressively increasing displacement amplitude were applied before the FME was reached. Subsequent loading followed the Sequential Phase Displacement (SPD) procedure which involves application of degradation and stabilization cycles at a constant displacement amplitude before progressing to the next phase with a greater displacement. The first cycle in a phase is applied with a larger displacement, and is proceeded by three degradation cycles; subsequent application of three stabilization cycles completes the phase. Stabilized response is achieved when the decrease in resistance between two successive stabilization cycles is less than 5% (Soudki, West et al. 1996). If the decrease in resistance is more than 5%, additional stabilization cycles should be conducted. The frame tested in this study stabilized in five cycles. The procedure then moves on to the next phase (Salenikovich, Dolan et al. 1999, Gatto and Uang 2003, Ibarra, Medina et al. 2005).

Cyclic testing of the frame was performed in accordance with ASTM E2126 Method A, that closely follows the SPD procedure developed by TCCMAR (Porter 1987) with few modifications. The SPD procedure is based solely on the First Major Event (FME), where FME is defined as the displacement at which the structure starts to deform inelastically (anticipated yield displacement) (Krawinkler 2009). ASTM E2126, on the other hand, takes into account both FME and ductility ratio when determining the initial amplitude of each phase in the test protocol. In general, the SPD protocol is displacement-controlled, and involves triangular reversed cycles at increasing displacement levels. The displacement increase in ASTM E2126 is based on FME and ductility ratio. The SPD procedure begins with at least three incremental levels of three cycles each, within the elastic displacement region up to the First Major Event (FME). The SPD method recommends 200% of the FME as the displacement increment for each phase in the case of ductile systems (Salenikovich, Dolan et al. 1999, Gatto and Uang 2003). The test protocol devised here, based on ASTM E2126 requirement, comprised 15 steps of displacement increase, with trailing cycles after each peak cycle as shown in Table 11.

Table 11. Test protocol for evaluation of the frame performance under cyclic lateral loads

Load step	Drift	Peak Displacement, cm	Trailing Cycle Displ.	# of trailing cycles
1	0.050%	0.048	0.048	5
2	0.075%	0.072	0.054	6
3	0.100%	0.096	0.072	6
4	0.20%	0.192	0.144	3
5	0.3%	0.288	0.216	3
6	0.4%	0.384	0.288	3
7	0.7%	0.672	0.504	2
8	1.00%	0.960	0.720	2
9	1.50%	1.440	1.080	2
10	2.00%	1.920	1.440	2
11	2.50%	2.400	1.800	2
12	3.00%	2.880	2.160	2
13	4.00%	3.840	2.880	2
14	4.50%	4.320	3.240	2
15	5.00%	4.800	3.600	2

5.3 Experimental Results

5.3.1 Aerated Slurry-Infiltrated Chicken Mesh Sheets

Typical flexural load-deflection curves for the aeriated slurry-infiltrated chicken mesh sheets are presented in Figure 51. The flexural behavior is observed to be ductile. Specimens with lower chicken mesh ratios produce lower flexural strengths. The sheet with 12 layers of chicken mesh reinforcement (and 25.4 mm thickness) provided the highest peak load of 2.2KN. Figure 12a shows a typical sheet specimen after flexural failure. Typical crack patterns underneath the test specimens are shown in Figure 52b. Failure exhibited a somewhat distributed nature.

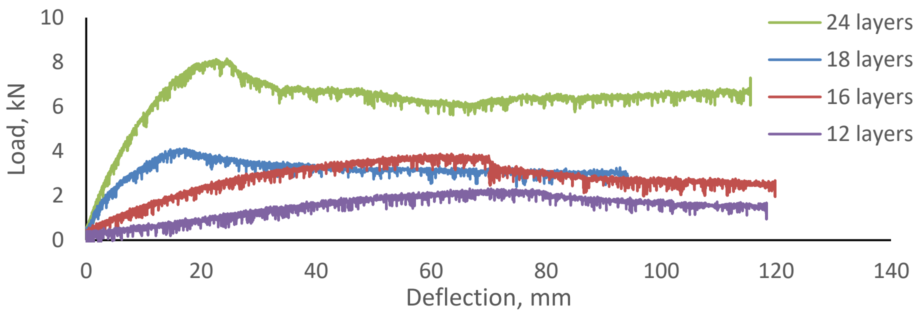

Figure 51. Flexural load-deflection behavior of aerated slurry-infiltrated chicken mesh sheets

Figure 52. Aerated slurry-infiltrated chicken mesh sheet after flexural failure.

Figure 53 shows the load-deflection curves obtained in two punching shear tests performed on aerated slurry-infiltrated chicken mesh sheets with different numbers of chicken mesh layers. The sheets with 12 and 16 layers of chicken mesh were 25.4 and 31.75 mm thick, respectively. The peak load in punching shear increased with increasing number of chicken mesh layers (which accompanied increasing thickness), and the behavior was ductile. Both specimens performed favorably in punching shear; the loaded area could not penetrate through the sheet specimen even after 45 mm of displacement. The chicken mesh reinforcement effectively mitigated penetration of the small loaded area into the sheet (Figure 54).

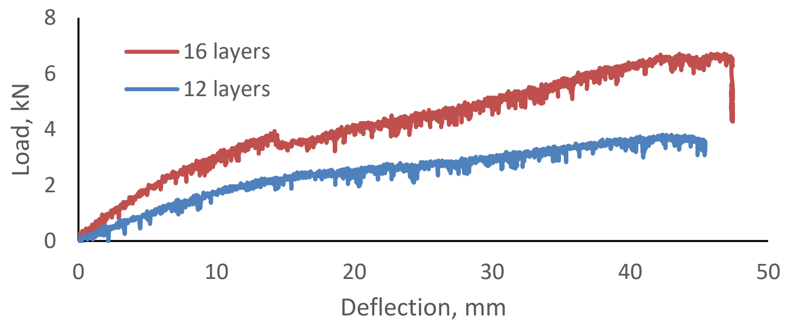

Figure 53. Punching shear load-deflection curves

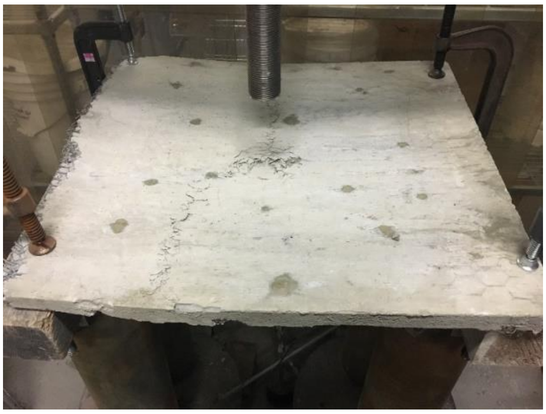

(a) Failed specimen

(b) Failure mode underneath the loaded area

Figure 54. Typical failure mode of aerated slurry-infiltrated chicken mesh sheets subjected to punching shear.

5.3.2 Aerated Slurry-Infiltrated Chicken Mesh Beams

A beam test specimen under flexural loading is shown in Figure 55a. Failure of aerated slurry-infiltrated chicken mesh beams involved multiple cracking over an extended length of the beam. Figures 55b and 55c shows the load-deflection behavior of the two beams tested in this experimental program. Failure was highly ductile, with the peak load retained over large deformations. The nature of tensile failure in aerated slurry-infiltrated chicken mesh beam was different from those observed in reinforced concrete. Besides the formation of closely spaced multiple cracks, a tendency towards crushing of the aerated slurry was also noted, which could be attributed to the bearing action of the chicken mesh wires against aerated slurry. Given this failure mode, one of the beams was subjected to reverse loading (Figure 56a) after failure under original loading in order to gain an initial insight into its cyclic behavior. As shown in Figure 56b, the peak load under reverse loading approached that under the original loading direction.

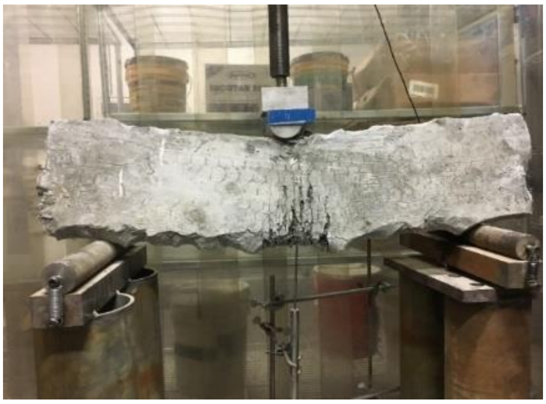

(a)

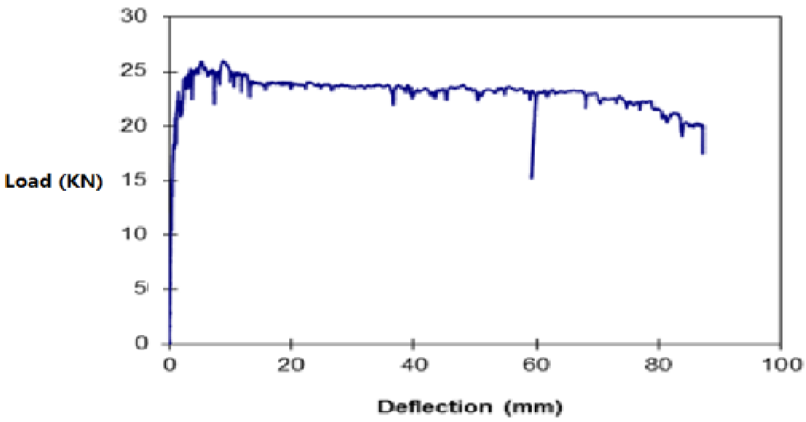

(b)

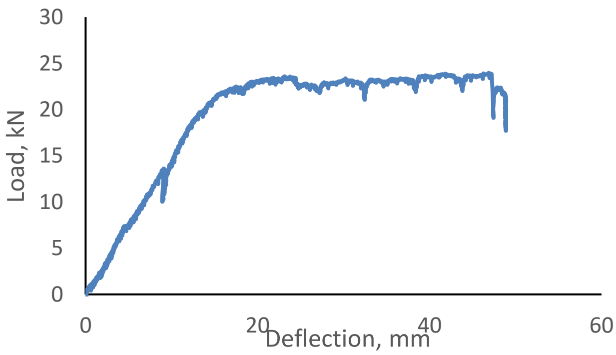

(c)

Figure 55. Flexural behavior of aerated slurry-infiltrated chicken mesh beams: (a) typical failure mode; (b) & (c) flexural load-deflection behavior of two beams.

(a)

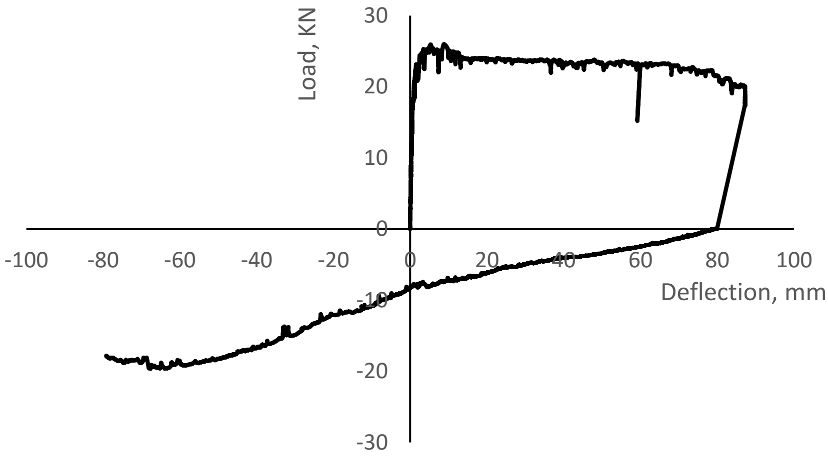

(b)

Figure 56. Flexural behavior under reversed loading: (a) test setup; (b) load-deflection behavior.

Under shear loading, aerated slurry-infiltrated chicken mesh exhibited high strength levels (about five times that obtained in flexure). The shear failure mode and load-deflection behavior are shown in Figure 57. Besides a high shear strength, the beam also failed in a ductile manner in shear. The distinctly favorable shear behavior of aerated slurry-infiltrated chicken mesh can be attributed to: (i) the dual role of chicken mesh, which is distributed across the thickness as both flexural and shear reinforcement; (ii) the highly ductile behavior of aerated slurry-infiltrated chicken mesh in shear; and (iii) the high specific surface area of the chicken mesh wires which benefits their dowel action against the aerated slurry.

(a)

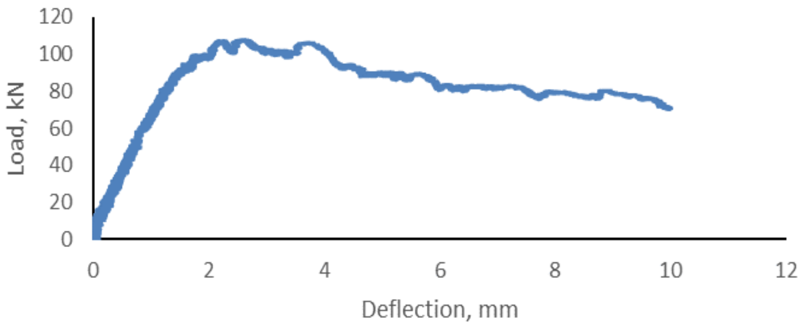

(b)

Figure 57. Shear behavior of an aerated slurry-infiltrated chicken mesh beam: (a) failure mode; and (b) load-deflection behavior.

5.3.3 Aerated Slurry-Infiltrated Chicken Mesh Columns

Figure 58 presents a typical compressive stress-deflection behavior for an aerated slurry-infiltrated chicken mesh column. A peak stress of 15 MPa was reached, noting that loading had to be discontinued due to deflection limitations of the test setup in the midst of an extended strain-hardening behavior of the column. The column behavior in compression was highly ductile, with a strain-hardening behavior which could be attributed to the confining effects of chicken mesh on the aerated slurry (which also mobilizes the lateral tensile behavior of the chicken mesh layers restrained by the aerated slurry). It should be noted that the aerated slurry provided only 5.4 MPa compressive strength.

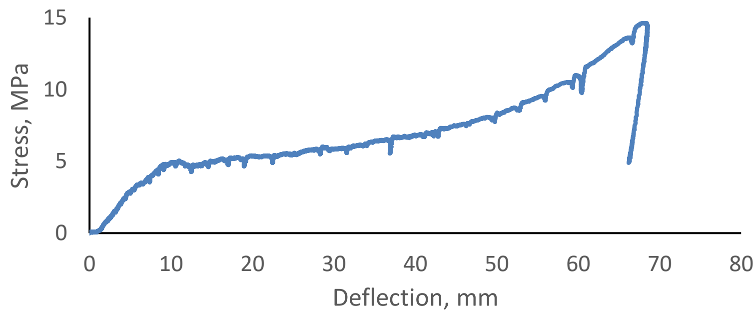

Figure 58. A typical compressive stress-deflection behavior of aerated slurry-infiltrated chicken mesh.

5.3.4 Aerated Slurry-Infiltrated Chicken Mesh Subcomponents

Figure 59a shows the load-deflection behavior of a subcomponent comprising an aerated slurry-infiltrated chicken mesh frame to which two aerated slurry-infiltrated chicken mesh sheets were nailed, and was subjected to cyclic in-plane lateral loading. Figure 59b shows the lateral in-plane load-deflection behavior of a similar frame tested alone (without any sheets nailed to it). Due to some constraints in loading frame geometry, cyclic loading could not be applied symmetrically. Nailing of sheets to the frame increased their lateral load-carrying capacity by more than 50%. Frames with and without nails both exhibited ductile behavior with desired hysteretic energy absorption capacity under lateral in-plane loading, noting that the hysteretic curves were somewhat pinched in both cases. The frames tested here had relatively high height-to-width ratios of 1 (compared to 0.5 for the actual building). This particular geometry produced a tendency towards tensile failure of the column at its base in lieu of plastic hinge formation in the beam(Figure 60). This failure mode, however, did not compromise the ductility and hysteretic energy absorption capacity of the frame and the subcomponent due to the ductile behavior of aerated slurry-infiltrated chicken mesh under all loading conditions. The nails experienced some cyclic lateral deformations when the subcomponent was subjected to cyclic in-plane loading.

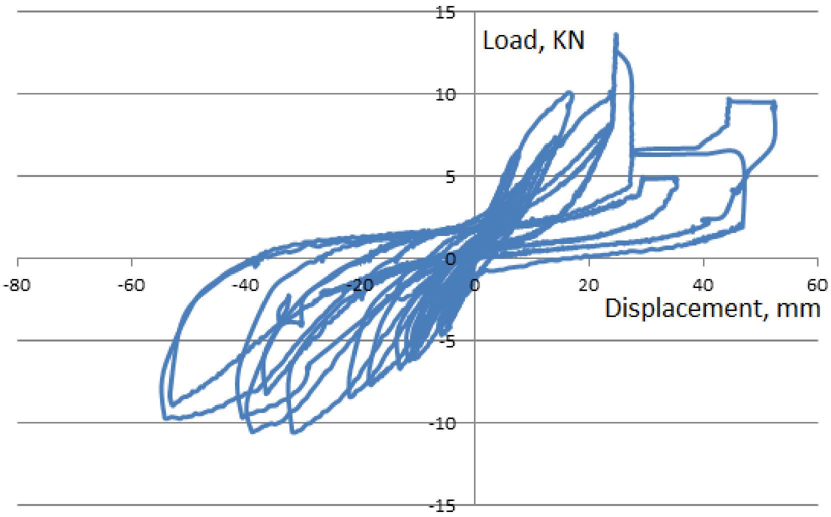

(a) Frame with nailed sheets

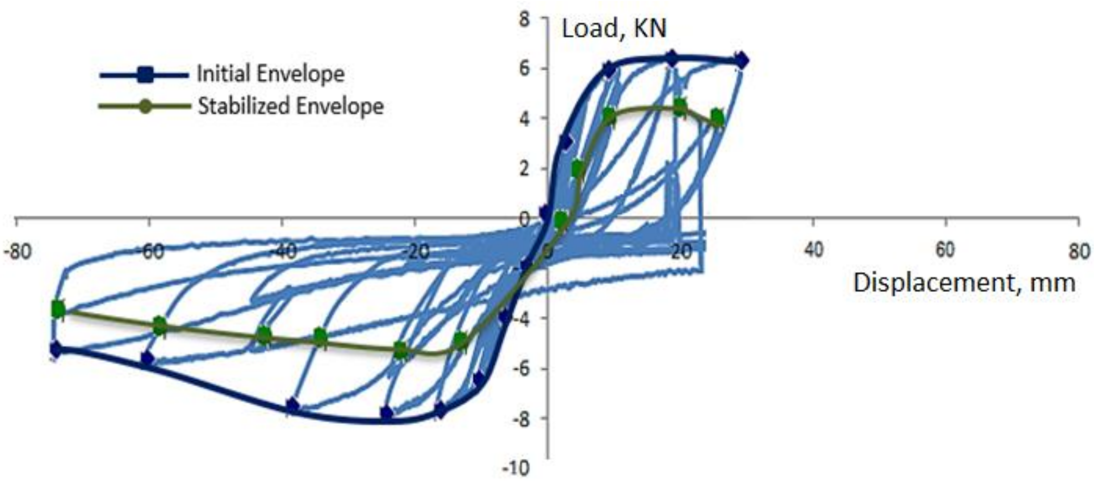

(b) Frame without nailed sheets

Figure 59. Hysteretic in-plane behavior of aerated slurry-infiltrated chicken mesh frame with and without nailed sheets.

(a) Tensile failure of a column

(b) Cyclic lateral deformations of a nail

Figure 60. Failure modes of the subcomponent comprising a frame with two sheets nailed to it.

The larger building subcomponent comprising two frames as well as interior and exterior wall and ceiling/roof sheets nailed to it was subjected to cyclic lateral loading applied perpendicular to the plane of frames. This building provided a desired balance of strength, ductility and hysteretic energy absorption capacity (Figure 61). The nails joining the sheets to frames played a prominent role in resisting lateral loads, noting that the frame has limited load-bearing capacity when lateral loads are applied normal to their planes. The subcomponent behavior under lateral loading is shown in Figure 62. Nails kept the original wall orientation, and lateral deformations were allowing by nails deforming laterally into the aerated slurry-infiltrated chicken mesh sheets. Effective interactions of nails with chicken mesh layers explain the desired lateral load-deflection behavior of this building subcomponent.

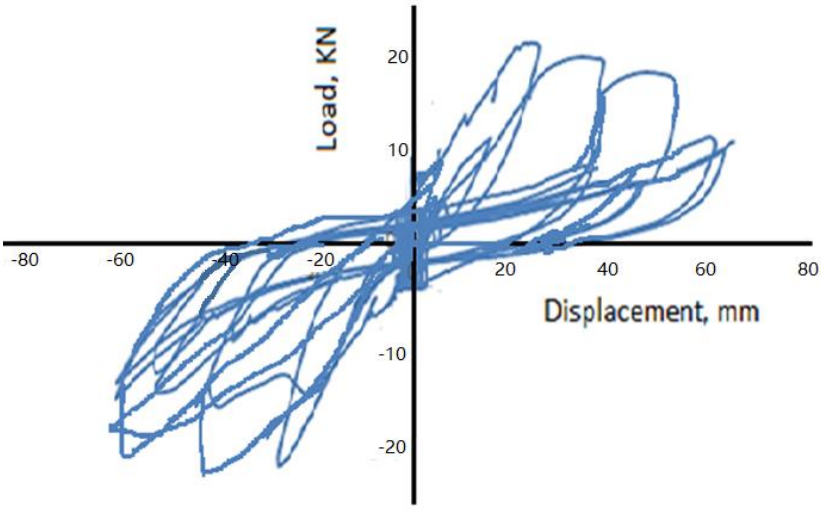

Figure 61. Hysteretic behavior of the aerated slurry-infiltrated chicken mesh building subcomponent comprising two frames with interior and exterior wall and ceiling/roof sheets nailed to it, and subjected to cyclic lateral loading perpendicular to the plane of frames.

Figure 62. Failure modes of the subcomponent comprising two frames with sheets nailed to their interior and exterior, and loading applied perpendicular to the frame planes.

CHAPTER 6
STRUCTURAL DESIGN OF A LIGHTWEIGHT BUILDING SYSTEM MADE WITH LOCALLY AVAILABLE MATERIALS

6.1. Introduction

The design loads of aerated slurry-infiltrated chicken mesh buildings were decided. The critical factored load combinations were identified. The aerated slurry-infiltrated chicken mesh frames, wall and roof/ceiling sheets, floor panels, and screws were designed to safely resist the governing load combinations.

6.2. Design Loads

Design loads were defined for the indigenous B-Hut. The live and snow loads were similar to those used with conventional B-Huts. Dead loads were determined considering the densities and dimensions of the indigenous building materials and components developed in the project. Relatively high seismic load were selected, relying upon the highly ductile behavior of the indigenous building materials developed in the project to absorb the input energy of strong earthquakes. In the short direction, frames are responsible for resisting seismic forces. Procedures were devised for design of indigenous (aerated slurry infiltrated chicken mesh) frames under seismic and gravity loads. Indigenous frames were designed to meet the structural requirements without exceeding weight limits that allow for manual installation of the indigenous B-Hut. These dimensions also suit thermal insulation of the roof and walls.

6.2.1 Roof Loads

The roof loads were selected to match those used for conventional B-Hut design:

Live load: 20 psf

Snow Load: 42 psf

The roof-level dead load comprises masses of: (i) roof sheets that are 25.4 mm thick with 0.9 bulk specific gravity; (ii) ceiling sheets that are 19 mm thick with 0.75 bulk specific gravity; (iii) beams that are 9 in high and 4 in wide with bulk specific gravity of 0.75, with 4 ft spacing.

The contributions of various components to the roof-level mass are as follows: (i) 4.667 psf from roof sheets; (ii) 2.925 psf from ceiling sheets; and (iii) 2.925 psf from beams. The total roof-level dead load adds up to 10.517 psf.

The vertical component of seismic force is considered to be equal to the roof dead load times two-thirds of the horizontal acceleration used in seismic design (described below).

6.2.2 Floor Loads

The floor live load used in B-Hut design is 60 psf. In order to control floor deflections (a serviceability issue), a concept that is somewhat similar to slab-on-grade is used for floor design. Compacted sand provides the grade upon which one layer of aerated slurry-infiltrated chicken mesh sheets will be placed. The sand layer will be covered with a plastic sheet for sealing purposes. Considering the 1 inch thickness for the aerated slurry infiltrated chicken mesh floor sheets of 0.9 bulk specific gravity (and 1.75 bulk specific gravity of compacted sand), the floor dead load can be calculated at 25 psf. This load is a consideration in floor design, but does not contribute to the seismic forces applied to the building structure.

6.2.3 Seismic Forces (Base Shear Method)

The seismic forces acting on the building were calculated following the ASCE-07 procedures. The maximum earthquake ground motion considered was defined by:

$S_s = 3.4$

$S_1 = 1.6$

where, S_s and S_l are the spectral accelerations defining the design response spectrum.

Table 12 presents the values of F_a (short-period site coefficient) associated with a standard “firm” soil condition used in residential building design. F_a values decrease with increasing ground motion because the soil begins to dampen the ground motion as shaking intensifies. Therefore, soil can have a moderating effect on the seismic shear loads experienced by the buildings in high seismic risk regions. Dampening also occurs between a building foundation and soil, and thus has a moderating effect.

Table 12. Site soil amplification factor relative to acceleration (short period, firm soil).

S_s	≤ 0.25g	0.5g	0.75g	1.0g	≥ 1.25g
F_a	1.6	1.4	1.2	1.1	1.0

Calculation of the seismic force is outlined below.

Site class is considered to be D (stiff soil):

F_a=1.1 & F_v=1.5

Adjusted maximum earthquake response acceleration:

S_{MS}= $(F_a)(S_s)$=3.74 g

S_{M1}=$(F_v)(S_1)$=2.4 g

Design spectral response acceleration:

S_{DS}= (2/3) S_{MS}=2.5 g

S_{D1}= (2/3) SM_1=1.944 g

Calculation of the seismic response coefficient is described below.

Considering that some buildings can effectively dissipate energy from seismic ground motions through ductile (damaging) behavior, the R factor is used to adjust the shear forces that would have been experienced by a building exhibiting a perfectly elastic behavior without some form of ductile energy dissipation. The concept has served a major role in standardizing the seismic design of buildings even though it has evolved in the absence of a repeatable and generalized evaluation methodology with a known relationship to actual building performance. Those structural building systems that can withstand greater ductile damage and deformation without substantial loss of strength are assigned a higher value of R. The R factor also reflects the differences in damping effects that are believed to be exhibited by various structural systems. Table 13 presents some R values that are relevant to residential construction.

Table 13. Seismic response modifier (R) values for residential construction.

Structural System	Seismic Response Modifier, R
Light-frame shear walls with wood structural panels used as bearing walls	6.0
Light-frame shear walls with wall board/lath and plaster	2.0
Reinforced concrete shear walls	4.5
Reinforced masonry shear walls	3.5
Plain concrete shear walls	1.5
Plain masonry shear walls	1.25

The indigenous building system developed in this project, where aerated slurry-infiltrated chicken mesh is used as structural material, exhibits a distinct ductile behavior when subjected to different force systems (even shear). The structural system also relies upon the hysteretic behavior of screws acting laterally against aerated slurry-infiltrated chicken mesh sheets to dissipate the seismic energy input. The screw behavior in this mode of action is also highly ductile, with highly desired hysteretic energy absorption capacity (in spite of the pinched nature of the hysteretic curves). Considering the unusually high ductility and energy dissipation capacity of aerated slurry-infiltrated mesh structural systems and their (screwed) joint, a high R value of 9 was considered in seismic design of the indigenous building systems developed in the project.

An occupancy importance factor of I=1 was used in the indigenous B-hut design.

The value of C_s can thus be calculated as follows:

$$C_s = \frac{S_{Ds}}{R/_I} = 0.267$$

The maximum seismic response coefficient is:

C_t=0.028, x=0.8

The fundamental period of vibration (T) can be estimated as:

$T_a = C_t h_n^x = 0.028*(10)^{0.8} = 0.17$ sec

$T = C_u T_a = 1.4*0.17 = 0.227$ sec

The value of $C_{s,max}$ can be calculated as follows:

$$C_{s,max} = \frac{S_{D1}}{T\,(R/_I)} = \frac{1.944}{0.227*^{9.37}/_1} = 0.85 \text{ g}$$

For category II, the minimum seismic response coefficient is:

$$C_s = \frac{0.5\,S_1}{R/_I} = \frac{0.5*1.944}{9.37/1} = 0.104 \text{ g}$$

Hence, $C_s = C_{s,max} = 0.85$ g

The vertical component of the design acceleration is estimated at (2/3).$C_{s,max}$ = 0.566 g.

The building mass can be divided into two components concentrated at: (i) roof level, comprising roof and ceiling sheets, strips sealing these sheets, and beams; and (ii) wall level, comprising interior and exterior sheets, and columns. The corresponding seismic forces are thus applied at the roof level and the mid-height of the building (Figure 63).

Figure 63. Seismic forces applied at two levels: roof and mid-height.

The seismic force applied at the top level (F_t) is 2.6 times the roof-level dead load:

F_t = 0.85 x (10.517 psf) x (18 ft) x 34 ft) = 0.85 x 6436.4 = 5,470 lb

The seismic force applied at mid-height (F_m) is 2.6 times the dead load associated with wall sheets and columns. All aerated slurry-infiltrated chicken mesh sheets are assumed to have a thickness of ¾ in. The bulk specific gravities of external and internal sheets are 0.9 and 0.75, respectively. The columns of frames are 10.5 in high and 4 in wide, with a bulk specific gravity of 0.9 the total number of columns is 18, and the internal and external sheets cover surface areas close to 800 sq ft (each). The total weight of wall sheets and columns thus add up to 5,150 lb (wall sheets) plus 1,966 lb (columns). The seismic force applied at mid-height (F_m) it thus:

F_m = 0.85 x (5,150 + 1,966) = 0.85x 7,116 = 6,048 lb

The above horizontal seismic forces can be applied in either the short or the long direction of the building.

The out-of-plane seismic forces applied to interior and exterior wall sheets are as follows:

Interior Sheets: 0.85 x 2.93 = 2.49 psf

Exterior Sheets: 0.85 x 3.51 = 2.98 psf

Design of wall sheets under out-of-plane forces would be governed by above forces. The pullout resistance of the wall sheet screws should also be adequate to resist these forces.

In the short direction, horizontal seismic forces should be resisted by the frames (Figure 64a, which also show the wall, roof, ceiling and floor aerated slurry-infiltrated chicken mesh sheets to be screwed to frames). The building frame overall and cross-sectional dimensions are presented in Figure 64b. The cross-sectional dimensions were derived following trial-and-adjustment procedures which accounted for the weak beam–strong column requirement. It should be noted that the frames were actually made with aerated slurry-infiltrated chicken mesh prepared with an aerated slurry of 0.75 bulk specific gravity.

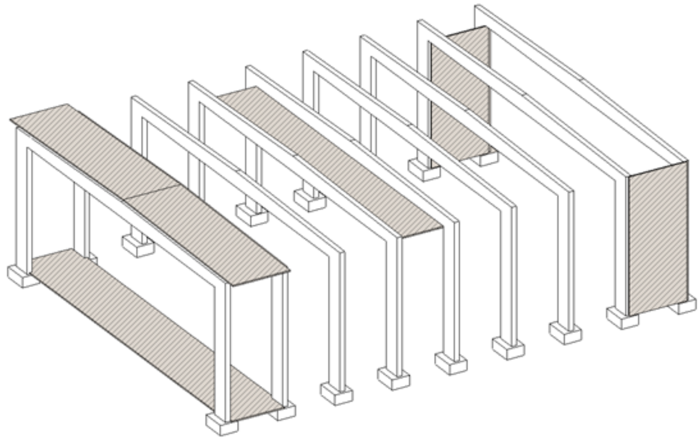

(a) Overall view of the building frames

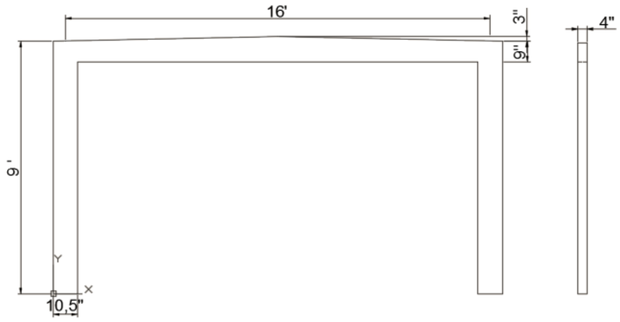

(b) The frame geometry and cross-sectional dimensions

Figure 64. Building frames.

6.3. Structural Analysis and Design of Building Frames

6.3.1 Structural Analysis of Building Frames

The indigenous building comprises 9 frames, with a total of 18 columns. The maximum bending moment generated under horizontal seismic forces at the column base can be calculated (Figure 65) as:

$$M = [F_t.h + F_m.(h/2)]/9 = [5{,}470 \text{ lb x } 8 \text{ ft} + 6{,}048 \text{ lb x } 4 \text{ ft}]/18 = (43{,}760 + 24{,}102)/18$$

$$= 3{,}700 \text{ lb.ft}$$

The base shear force applied to each column can be calculated as follows:

$$v = (F_t + F_m)/18 = (5{,}470 + 6{,}048) / 18 = 639 \text{ lb}$$

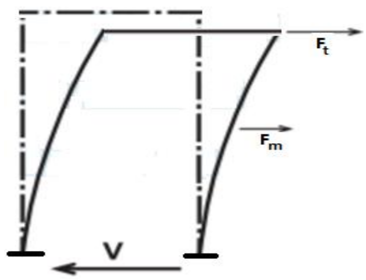

Figure 65. Deformation of a building frame subjected to horizontal seismic forces in the short direction of the building.

The vertical component of the seismic force, estimated at two-thirds of the horizontal component, could influence the roof (and ceiling) design. The downward component of this force plus the force of gravity would be (0.566 + 1) x 10.517 = 16.46 psf. The upward component of this force minus the force of gravity would be (0.566 – 1) x 10.517 = -4.56 psf. The downward out-of-plane seismic force associated with the mass of (interior) ceiling sheets is (0.566 + 1) x 2.925 psf = 4.58 psf. This force would govern the out-of-plane design of the ceiling sheets and their screws. The critical out-of-plan force of (exterior) roof sheets is upward, and is equal to (0.566 – 1) x 4.667 = -2.02 psf. This pullout resistance provided by screws should be adequate to resist this force. Design of roof sheets for out-of-plane behavior should be based on the heavier snow loads.

Snow load is larger than the vertical component of seismic force. Therefore, the maximum internal forces developed in the building frame would result from load combinations including the snow load. Among the factored load combinations involving snow load, that with the highest factor for snow load governs the design for gravity loads:

U = 1.2 D + 1.6 S = 1.2 (10.517) + 1.6 (42) = 12.62 + 67.2 = 79.82 psf

Each frame has a tributary width of 4 ft. (see Figure 2a). Therefore, the factored gravity load applied to the beam of the frame can be estimated as:

w = 4 x 79.82 = 319.28 lb/ft

The maximum bending moment developed in the beam under vertical loads could be estimated as:

$M_u = 0.5xw.l^2/12 = 0.5x319.28 \times 16^2/12 = 3{,}403$ lb.ft

This bending moment is less than (but close to) that produced under the horizontal component of seismic load. Seismic forces thus provide the basis for design of the beam. The beam midspan would develop (under snow and dead loads) a factored bending moment that is close to that developed at the beam ends under the horizontal component of seismic load. Aerated slurry reinforced chicken mesh would provide comparable flexural strengths at midspan and at ends. Therefore, the design for the horizontal component of seismic load would also ensure safety under the critical (snow plus dead) vertical load.

Structural Design of the Building Frames

The tensile and compressive strengths of aerated slurry-infiltrated chicken mesh were derived semi-empirically. In tension, any direct contributions of the aerated slurry to tensile strength were neglected. The aerated slurry, however, makes significant indirect contributions to tensile strength by restraining the chicken mesh wires (which are partly oriented at an angle with respect to the tensile stress orientation) from realignment to get oriented parallel with the tensile stress direction. The tensile strength of aerated slurry-infiltrated chicken mesh was expressed as follows:

$$\sigma_T = \alpha \rho f_y$$

where, σ_T = tensile strength of the aerated slurry infiltrated chicken mesh, ρ = area ratio of the chicken mesh wires oriented at less than 90° with respect to the tensile stress direction, f_y = yield stress of the chicken mesh wires (310 MPa), and α = an empirical efficiency factor which reflects partial reorientation of a fraction of chicken mesh wires and the effectiveness of the restraining effect of the aerated slurry matrix against reorientation of these wires along the tensile stress direction; the value of α was found to be 0.56 based on experimental results.

In compression, the composite behavior of aerated slurry-infiltrated chicken mesh produces a compressive strength that can be expressed as follows:

$$\sigma_C = \beta\rho f_y + \gamma f_c'$$

where, σ_c = compressive strength of aerated slurry-infiltrated chicken mesh, β = efficiency factor of chicken mesh reinforcement in compression (it was assumed to be similar to the efficiency factor of chicken mesh in tension, that is 0.56), and γ = efficiency factor of the aerated sully in compression, which was surprisingly found (based on test results) to be 4.6. In other words, the aerated slurry, when used with chicken mesh reinforcement, provides 5 times the compressive strength of plain aerated slurry. Different factors could contribute to the rise in the compressive strength of the aerated slurry in the presence of chicken mesh reinforcement, including: (i) the relatively low elastic modulus and high Poisson's ratio of the aerated slurry are expected to produce relatively large strains in compression which are restrained by the chicken mesh reinforcement of high specific surface area and close spacing, with the resulting confining effect raising the aerated slurry compressive strength; and (ii) chicken mesh with high specific surface area and close wire spacing effectively reinforces chicken mesh against restrained shrinkage microcracking. The rise in compressive strength of aerated slurry when used with chicken mesh reinforcement is a significant factor enabling the otherwise non-structural (insulating) aerated slurry to make structural contributions to the aerated slurry-infiltrated chicken mesh performance.

Using concepts similar to those used with reinforced concrete, the nominal flexural strength (M_n) of an aerated slurry-infiltrated chicken mesh cross-section (Figure 66) can be expressed as follows:

$$M_n = \alpha\rho f_y b(h - a)(\frac{h}{2})$$

where, ‘a’ is a value related to (and somewhat smaller than) the depth of neutral axis (c); a constant compressive stress is assumed up to depth ‘a’ in order to simulate the nonlinear compressive strength distribution up to the depth of neutral axis ‘c’. The value of ‘a’ can be derived based on the equilibrium of the tensile and compressive forces generated at the section subjected to bending moment:

$$\alpha\rho f_y(h-a) = \left(\beta\rho f_y + \gamma f_c'\right)a$$

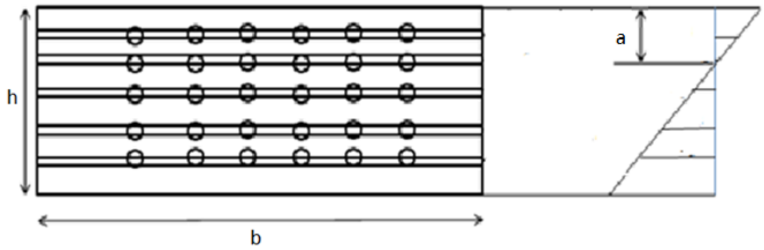

Figure 66. Cross-section and flexural strain distribution of aerated slurry-infiltrated chicken mesh.

As a first step, the expression derived above for the nominal flexural strength of aerated slurry-infiltrated chicken mesh was verified using experiments performed on a beam and a sheet made with aerated slurry-infiltrated chicken mesh sheets and beams. These structural test specimens were made with a slurry proportioned with saponin: water: cement at 0.00045: 0.6: 1 weight ratios (which yielded a bulk specific gravity of 0.8 after hardening and air-drying). Twelve layers of chicken mesh were used in the aerated slurry infiltrated chicken mesh sheet with a thickness of 20 mm. The resulting wire area ratio at the sheet cross section was 0.02. Table 14 presents the aerated slurry reinforced chicken mesh sheet dimensions, reinforcement conditions, test results, and the experimental and theoretical values of flexural strength. The theoretical values of flexural strength obtained with the expression presented above are observed to exceed experimental values by 2 to 7%. The approach outlined above for calculation of the nominal flexural strength of aerated slurry-infiltrated chicken mesh sheets and beams was thus considered to be valid.

Table 14. Aerated slurry infiltrated chicken mesh sheet and beam dimensions, reinforcement and loading conditions, and test results versus predicted values.

Specimen	# of Chicken Mesh Layers	Span, mm	Width, mm	Thickness, mm	Peak Load, N	3 or 4 Point Loading	Flexural Strength, N.mm	
							Test	Theory
Sheet	12	450	150	20	1300	4	97.5	94.2
Beam	30	800	102	254	25000	3	5000	5001

The aerated slurry-infiltrated chicken mesh beam and column cross-sections that meet the flexural strength requirements (governed by seismic loads) are shown in Figure 67. There are two groups of chicken mesh: (i) 30 layers which are placed in formwork in folded form; and (ii) four layers that are wrapped around to mitigate the potential for split cracking upon screw application to columns and beams. Along the height, the total number of chicken mesh layers is thus 38. Longitudinally and transversely oriented chicken mesh layers would produce 2.58% and 0.612% area fraction, respectively. In a later modification of the chicken mesh placement method, the mesh was formed via rolling rather than folding. This approach produced outer layers of chicken mesh that were parallel to the beam (and column) outer surfaces. Therefore, there was no need to have another groups of wire mesh to wrap the interior layers.

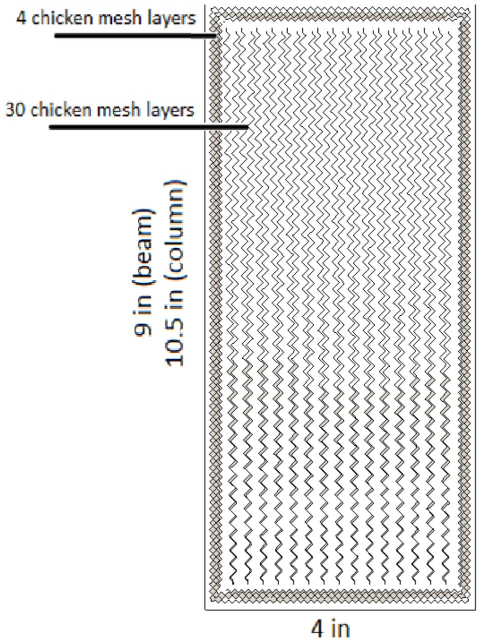

Figure 67. Aerated slurry infiltrated chicken mesh beam and column cross sections in building frames.

With longitudinally oriented chicken mesh layers, the tensile and compressive strengths of aerated slurry- infiltrated chicken mesh beams would be:

$\sigma_T = \alpha\rho f_y = 0.26x0.0258x310 = 2.08\ MPa$ (301.7 psi)

$\sigma_C = \beta\rho f_y + \gamma f_c'$ = 0.26x0.0258x310 + 4.6x3.5 = 18.18 MPa (2,637 psi)

Equilibrium of tensile and compressive forces can be used to calculate the value of 'a' required for calculation of the nominal flexural strength:

$\sigma_C . a = \ \sigma_T . (h - a)$

2,637xa = 301.7x(9-a)

a = 0.92 in

The nominal flexural strength of the aerated slurry-infiltrated chicken mesh can now be calculated as follows:

$M_n = \alpha\rho f_y b(h - a)(\frac{h}{2})$ = 0.26x0.0258x44,962x4x(9-0.92)x(9/2) = 44,607 lb.in

This nominal flexural strength of 44,607 lb.in (3,717 lb.ft) times capacity reduction factor (assumed 0.95 for the highly ductile aerated slurry-infiltrated chicken mesh) is adequate for resisting the maximum bending moment of 3,700 lb.ft developed under the horizontal component of seismic load and 3,403 lb.ft developed under the critical (factored snow plus dead) factored vertical load. The beam design is thus satisfactory as far as flexural forces are concerned.

The maximum shear force developed at the base of a column under the horizontal component of seismic load is 639 lb. The maximum shear force developed in beams under factored snow plus dead loads is (331 lb/ft)x(16 ft) / 2 = 2,648 lb. This maximum shear force in beams produces a shear stress of 2,648 / (4x9) = 73.6 psi. Mohr's diagram indicates that a diagonal tensile stress of about 73.6 psi would be developed as a result of this shear force. The tensile strength of the aerated slurry infiltrated chicken mesh sheet ($\sigma_T = \alpha\rho f_y$) in the longitudinal ($\rho$ = 0.0258) and transverse (ρ = 0.00612) directions are 302 psi and 71 psi. An average of these two values at 45o angle would be 187 psi. The critical tensile stress of 73.6 psi is thus significantly smaller than the nominal tensile strength (times a capacity reduction factor relevant to shear, which would be greater than 0.8 for the highly ductile aerated slurry infiltrated chicken mesh). The beam designed for flexure would thus behave safely in shear.

The critical axial force in columns would develop under factored snow plus gravity loads (82.176 psf). With a tributary width of 4 ft for each frame, this factored vertical force translates into a column axial force pf 81.176x4x18/2 = 2,922 lb. The resultant compressive stress developed in columns would be 2,922/(4x10.5) = 69.6 psi. The nominal compressive strength of the aerated slurry infiltrated chicken mesh column would be

$\sigma_C = \beta\rho f_y + \gamma f_c'$ = 0.26x0.0201x310 + 4.6x3.5 = 1.62 + 16.1 = 17.7 MPa (2,570 psi)

This nominal compressive strength (after application of a capacity reduction factor) would still be significantly greater than the maximum compressive stress developed in columns. The negligible compressive stress of columns implies that the design based on flexure is adequate.

The beam and column dimensions noted above produce a total frame weight of 389 lb (187 lb for the beam, and 202 lb for the two columns) that allows for its manual handling and assembly. These dimensions also provide the space required for insulation of the roof and walls.

6.3.2 Design of Roof Sheets

The aerated slurry infiltrated chicken mesh roof sheet that meet the flexural strength requirements have a thickness of 1 inch and 12 layers of chicken mesh reinforcement, with a width of 4ft and length of 9 ft that qualifies them as one-way slabs. The chicken mesh layers are oriented along the width of sheets (which is the direction of their one-way action).

For a 1-ft strop of sheet (b=1 ft) and the longitudinal direction of chicken mesh oriented along the width direction with 4 ft dimension. The tensile and compressive strengths of aerated slurry-infiltrated chicken mesh beams in the direction of one-way action would be:

$\sigma_T = \alpha\rho f_y = 0.26x0.0325x310 = 2.59\ MPa$ (375 psi)

$\sigma_C = \beta\rho f_y + \gamma f_c'$ = 0.26x0.0325x310 + 4.6x5 = 2.59 + 23.0 = 25.59MPa (3,711 psi)

Equilibrium of tensile and compressive forces can be used to calculate the value of ‘a’ required for calculation of the nominal flexural strength:

$\sigma_C . a = \sigma_T . (h - a)$

3,711xa = 375x(1-a)

a = 0.09in

Flexural strength of the aerated slurry-infiltrated chicken mesh roof sheet can now be calculated as follows:

$$M_n = \alpha\rho f_y b(h-a)(\frac{h}{2})$$ = 0.26x0.0325x44,962x12x(1-0.09)x(1/2) = 2074 lb.in

From ASD load Combinations and table 2, for a 1-ft width, the factored bending moment on the roof sheet is:

$M_u=ql^2/8=79.82 \times 4^2/8=159$ lb. ft=1907 lb.in

The nominal flexural strength of 2074 lb.in times the capacity reduction factor (assumed 0.95 for the highly ductile aerated slurry-infiltrated chicken mesh) is equal to the maximum factored bending moment of 1907 lb.in. The roof sheet design is thus satisfactory as far as the flexural forces are concerned.

6.3.3 Design of the Floor Sheets as Slabs-on-Grade

The k-value used for floor slab (sheet) design reflects the response of the subgrade under temporary (elastic) conditions and small deflections, usually 0.05 inches or less. Soil compressibility and bearing capacity values (normally used to predict and limit differential settlements between footings or parts of a foundation) reflect total permanent (inelastic) subgrade deformations that may be 20 to 40 (or more) times greater than the small deflections on which k-values are based. Substantial pavement research has shown that elastic deflections and stresses of the slab can be predicted reasonably well when using k-value to represent the subgrade response. Consequently, the control of slab stresses based on the subgrade k-value is a valid design procedure:

$$w = s\sqrt{\frac{kh}{E}}$$

where, w = the maximum allowable distributed stationary live load (60 pounds per square foot), s = allowable extreme fiber stress in tension (psi) excluding shrinkage stresses (assumed to be equal to one-half the normal 28-day flexural strength), k_s = the modulus of subgrade reaction (150 pounds per cubic inch for the conditions considered here), h = the slab (sheet) thickness (1 inch), E= elastic modulus of the slab (572,899 psi, 3.95 GPa).

$$60\ psf = 0.416psi = s\sqrt{\frac{\frac{150lb}{in^3}\times 1in}{572899psi}}$$

s = 25.7 psi

Hence, the required flexural (tensile) strength of the floor sheet is 2×s=51.4 psi.

The tensile strength provided by the aerated slurry-infiltrated chicken mesh sheet of 1 inch thickness with 12 layers of chicken mesh reinforcement is:

$\sigma_T = \alpha\rho f_y = 0.26x0.0325x310 = 2.59\ MPa$ (375 psi)

This value (even after application of a capacity reduction factor) would be an order of magnitude greater than the required level of tensile strength. Therefore, the floor slab (sheet) design is more than adequate for a slab-on-grade configuration.

The flexural strength of the floor sheet with 1 inch thickness and 12 layers of chicken mesh reinforcement is calculated below for a 1 ft strip

The aerated slurry-infiltrated chicken mesh floor sheet that meets the flexural strength requirements with 1 inch thickness, 4ft width by 16 ft length, 12 layers chicken mesh reinforcement.

The tensile and compressive strengths of aerated slurry infiltrated chicken mesh sheets would be:

$\sigma_T = \alpha\rho f_y = 0.26x0.0325x310 = 2.59\ MPa$ (375 psi)

$\sigma_C = \beta\rho f_y + \gamma f_c'$ = 0.26x0.0325x310 + 4.6x5 = 2.59 + 23.0 = 25.59MPa (3,711 psi)

Equilibrium of tensile and compressive forces can be used to calculate the value of 'a' required for calculation of the nominal flexural strength:

$\sigma_C.a = \sigma_T.(h - a)$

3,711xa = 375x(1-a)

a = 0.09in

Flexural strength of the aerated slurry-infiltrated chicken mesh sheet can now be calculated as follows:

$M_n = \alpha \rho f_y b(h-a)(\frac{h}{2})$ = 0.26x0.0325x44,962x12x(1-0.09)x(1/2) = 2074 lb.in

In case the slab (sheet) is subjected to four-point loading on a span of 16 ft without the benefit of the subgrade support, it can resist

$\mathrm{F} = 4xM_n x\frac{4}{L} = 4x2074lb.in\,x\frac{4}{16ftx12inch/ft} = 172\ lb$d*Approach for Foundation Design*

6.3.4 Footing Design

Figure 68 presents a schematic depiction of an isolated footing that resists forces generated in a column under gravity and lateral loads. The aerated slurry-infiltrated chicken mesh footing (Figure 69) that meets the strength requirements outlined below has a thickness of 8 in, planar dimensions of 14 in x 14 in, and 30 layers of chicken mesh reinforcement.

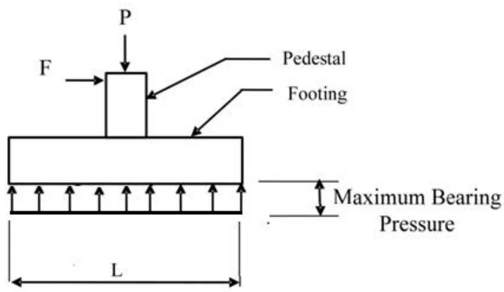

Figure 68. Schematics of the aerated slurry-infiltrated chicken mesh footing.

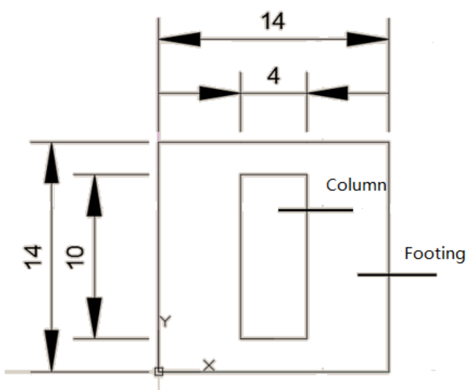

Figure 69. Top view of the footing.

Table 15 presents the presumptive soil bearing capacities for different soil types. B-Hut is assumed to be supported on a gravel, which provides a bearing capacity of 3,000 psf.

Table 15. Presumptive soil bearing values for different soil types.

Presumptive Load-Bearing Value (psf)	Soil Description
1,500	Clay, sandy clay, silty clay, clayey silt, silt, and sandy silt
2,000	Sand, silty sand, clayey sand, silty gravel, and clayey gravel
3,000	Gravel and sandy gravel
4,000	Sedimentary rock
12,000	Crystalline bedrock

The service loads that are transferred to the 18 isolated footings of the building are calculated below.

Floor Live load (16 ft)(32 ft)(60psf) = 30,720 lb

Floor Dead load (16 ft)(32 ft)(9psf) = 4608 lb

Footing and column dead load = 15729 lb

The minimum size of the concrete footing required to support the loads is:

The required soil bearing area = $\frac{Service\ load}{\text{Presumptive soil bearing capacity}}$

$$= \frac{(30{,}720+4608+15729)\text{lb}}{3000\text{ psf}} = 17\text{ ft}^2$$

The required bearing area for one isolated footing = 17 / 18 = 0.95 ft^2

Since the footing has a square planar geometry, the width will be b = $\sqrt{0.95} = 0.97$ ft = 12 in < 14 in

The soil pressure based on factored loads = q_s= $\frac{Pu}{A\,footing} = \frac{Dl+1.6}{17ft^2}$ = 2732 < 3000 psf , so the design is safe

For seismic flexural design

Seismic load E=8895 lb

1. Load= 1.4D=1.4 x4600=6,451.2lb

   6,451.2lb/(14^2*18)inch^2 =1.82psi=263.3psf

2. Load =1.2D+1.6L=1.2 x4600+1.6 x30720=54,681lb

   54,681lb/24.5ft^2=2231psf

3. Load= 1.2D+E+L=1.2 x4600+8895+30720=45,144lb

   45,144lb/24.5ft^2=1842psf

4. Load=0.9D+E= 0.9 x4600+8895=13,042lb

   13,042lb/24.5ft^2=532.2psf

The Load case 2 controls the flexural design for footing. The factored bending moment is:

$$M_u = q_u \left(\frac{l-c}{2}\right)^2 (b)/2$$

=2231psfx[(14inch-4inch)^2/2]x14inch/2/144ft^2/inch^2

=1355 lb. in

With longitudinally oriented chicken mesh layers in 4 ft direction, the tensile and compressive strengths of the aerated slurry-infiltrated chicken mesh sheet would be:

$\sigma_T = \alpha\rho f_y = 0.26x0.009x310 = 0.78\ MPa$ (113 psi)

$\sigma_C = \beta\rho f_y + \gamma f_c'$ = 0.26x0.009x310 + 4.6x3.5 = 0.78 + 16.1 = 16.88 MPa (2,448 psi)

Equilibrium of tensile and compressive forces can be used to calculate the value of ‘a’ required for calculation of the nominal flexural strength:

$\sigma_C . a = \sigma_T . (h-a)$

2,448xa = 113x(8-a)

a = 0.35 in

Flexural strength of the aerated slurry-infiltrated chicken mesh footing cross-section can now be calculated as follows:

$M_n = \alpha\rho f_y b(h-a)(\frac{h}{2})$ = 0.26x0.009x44,962x14x(8-0.35)x(8/2) = 45,072 lb.in

This nominal flexural strength times a capacity reduction factor (assumed to be 0.95 for the highly ductile aerated slurry-infiltrated chicken mesh) is significantly greater than the maximum bending moment of 1,355 lb.in. The footing design is thus satisfactory as far as flexural forces are concerned, noting that the transverse direction of chicken mesh would still provide adequate reinforcement and thus flexural strength.

6.3.5 Design of Screws

Different screws were evaluated for use with aerated slurry-infiltrated chicken mesh. These screws were 4 in long with 0.17 in or 0.14 in diameter, or 3 in long with 0.18 in or 0.11 in diameter.

The structural function of interior and exterior walls can be largely defined by their role in resisting lateral (seismic) forces in the direction that is out of the plane of frames. The screws joining the wall sheets to columns play a governing role in their design under seismic forces. The lateral seismic forces applied to interior and exterior wall sheets are as follows:

Interior Sheets: 0.85 x 2.93 = 2.49 psf

Exterior Sheets: 0.85 x 3.51 = 2.98 psf

The screws joining the exterior wall sheets to frames were designed under seismic loading. For the in-plane behavior of sheets under lateral loading, the required number of screws can be calculated as follows (Figure 70):

$$n = (P.H) / (F.b)$$

where, P (the lateral load apply on the top of frame) is 7585 lb, F (the nail effective plateau lateral load-carrying capacity) is 400 lb (from lateral nail resistance test), b is 16 ft, and H is 9 ft. The above equation thus yields n=10. Hence, 10 screws would be required for joining each side of a wall sheet to a column. The spacing between screws would be 10 in.

The pullout resistance of screws should also be adequate to resist the out-of-plane lateral force applied to wall sheets by the seismic inertia. The lateral load applied to a 4ft by 8 ft, external wall sheet with 1 in thickness is 2.98psf x4ft x8ft= 95.4 lb. The pullout resistance provided by one screw is 150 lb which is larger than the applied pullout force. Therefore, the number of screws required to join the wall sheets to columns would be governed by in-plane behavior. In order to improve the safety of screws design, it was decided to use 14 screws at 8 in spacing to join one side of a wall sheet to a column. The total number of screws required for joining of the internal and external wall sheets to frames would thus be 14 x2 x18 x 2=1008.

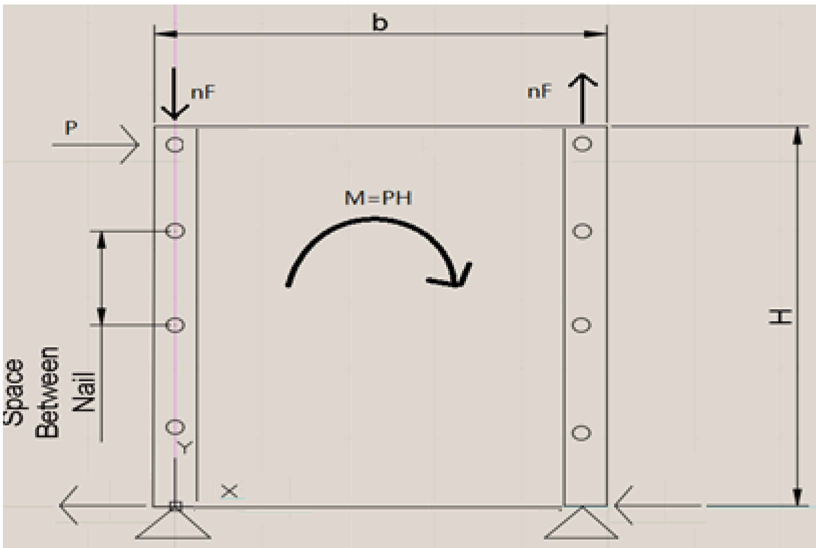

Figure 70. Forces transferred to nails under lateral loads applied in the plane of wall sheets.

For the roof and ceiling sheets:

$Cs = Cs_{max} = 2.6$ g

The in-plane lateral force applied to a 4ftx9ft roof sheet of 1 in thickness is 2.6 x4.667psf x4ft x9ft= 437 lb, which is comparable the 400 lb lateral load-carrying capacity of a screw applied to an aerated slurry-infiltrated chicken mesh sheet of 1 in thickness with 12 layers of chicken mesh reinforcement. The upward out-of-plane seismic force applied to a roofing sheet is (2.6-1) x4.667psf x4ft x9ft= 269 lb, which can be can be carried by the pullout resistance of two screws, noting that each screw provides

150 lb pullout resistance. Therefore, the demand on the pullout action of roof screws does not govern their design. Ceiling sheets with 4ftx8ft planar dimensions, 0.75 in thickness and 0.75 bulk specific gravity would place even less demand on screws joining them to beams. Roof and ceiling sheets provide for improved continuity of the building systems, and enable redistribution of forces in case one building frame or region experiences excess inelastic deformations. These important functions rationalize the choice of using a screw spacing of 8 in, similar to walls, for roof and ceiling sheets.

CHAPTER 7
DURABILITY OF AERATED SLURRY-INFILTRATED CHICKEN MESH

7.1. Introduction

Aerated slurry-infiltrated chicken mesh has been developed as a lightweight composite material for construction of safe, affordable, sustainable and economical buildings using locally available materials and resources. This composite material has been inspired by ferrocement, except that it is developed to meet greater structural demands. It incorporates higher volume fractions of finer reinforcement systems; the resulting congestion of reinforcement would require use of a highly flowable slurry to infiltrate the closely spaced reinforcing elements (wires) of high specific surface area. Another distinguishing feature of the new composite material involves use of aerated slurry with bulk specific gravities less than 1. Such lightweight cementitious materials are known to offer insulating by not structural qualities. It is the synergistic actions of the aerated slurry matrix and the fine (chicken mesh) reinforcement that transforms the aerated slurry into a structurally viable matrix, and effectively mobilizes the chicken mesh reinforcement qualities.

Aerated slurry-infiltrated chicken mesh offers constructability attributes which, to some extent, approach those of wood. Its moisture and moisture and weathering resistance, on the other hand, could approach those of concrete. These features allow for construction of the whole building, including the exterior (roof and wall) envelope of buildings, in addition to their structural and interior elements, with aerated slurry-infiltrated chicken mesh. In roofing and exterior wall applications, aerated slurry-infiltrated chicken mesh would be exposed to weathering effects. The work reported herein evaluated stability of this composite material under exposure to accelerated wetting-drying and freezing-thawing cycles. Standard accelerated aging methods developed for use with cementitious siding and roofing elements were used in this experimental program. The effects of accelerated aging on the aerated slurry-infiltrated chicken mesh sheets were evaluated through performance of flexure tests at different stages of aging.

7.2. Material and Methods

Saponin was used as a foaming agent, which is extracted from plants. The aerated slurry formulation used in this investigation comprised cement: water: saponin at 1: 0.6: 0.0005 weight ratios, which produced a bulk density of 0.8 g/cm^3 after curing and air-drying. A blend of saponin and mixing water was subjected to high-speed mixing; the resulting foamed mixing water was then mixed with cement in a mortar mixer. Sheet specimens of 500mmx500mm planar dimensions with 20 mm thickness and 12 layers of chicken mesh reinforcement were prepared by simply pouring the slurry on top of the chicken mesh layers; the flowable slurry infiltrated the chicken mesh and produce composite sheets. The sheets were moist-cured at >95% relative humidity and room temperature for 7 days, and then air-dried at 50±5% relative humidity for another 7 days. Three groups of sheets were prepared; one group were tested without exposure to accelerated aging after saturation via immersion in water at room temperature for 48 hours. The other two groups were subjected to repeated wetting-drying cycles and repeated freezing-thawing cycles following the procedures outline below.

ASTM C1185 and ASTM C1186 present requirements relevant to cementitious sheets used as the exterior envelope of building systems. The roofing sheets are subjected to more severe weathering effects than the exterior wall sheets (sidings). Therefore, the accelerated aging conditions recommended for roofing sheets were used in this experimental work.

7.2.1. Repeated Wetting-Drying Cycles

This accelerated aging condition simulates cyclic outdoor exposures involving rainy and sunny days. Figure 71 shows an aerated slurry-infiltrated chicken mesh sheet subjected to wetting (water spray) and (radiation) heating cycles. The sheet has the orientation of a roof, and is subjected to repeated cycles comprising four phases. These phases are: (i) water spray at a rate of 4 L/min for a period of 2 h 55 min, with a water temperature not exceeding 40°C (86°F); (ii) pause for a period of 5 min; (iii) radiant heating to raise the specimen surface temperature to 60±5°C for a period of 2 h and 55 min; and (iv) pause for a period of 5 min. The specimen is inspected visually after each cycle for finding any damage or structural alteration caused by the wetting-drying cycles; they are then subjected to flexure testing.

(a) (b)

Figure 71. Accelerated rain-heat exposure testing of a sheet specimen: (a) water spray; (b) radiant heating.

7.2.2. Repeated freezing-Thawing Cycles

In this accelerated aging process, the test specimens are first immersed in water at 16±10°C for a minimum of 48 h. They are then subjected to 50 cycles of freezing and thawing that comprise: (i) freezing at -23±6°C for a minimum of 1 h; (ii) thawing to reach a temperature of 16±10°C within 24 h; and (iii) holding for a minimum of 1 h. The freeze-thaw cycle time is 6 h. After finishing the cycles of freezing and thawing, the specimens are saturated by immersing in water at 15°C for 48 hours, and then subjected to flexure testing.

7.3. Test Results and Discussion

Exposure of aerated slurry-infiltrated chicken mesh sheets to wet-dry and freeze-thaw cycles did not produce any visible indications of damage (Figure 72). Table 16 and Figure 73 summarize the flexural strength test results for aerated slurry-infiltrated chicken mesh sheets in unaged condition and after exposure to different wetting-drying and freezing-thawing cycles. Analysis of variance of test results indicated that the effects of wetting-drying cycles on flexural strength are statistically negligible at 0.1% level of significance. The accelerated aging effects on flexural strength are relatively small, and are not statistically significant at 5% significance level.

(a) Unaged

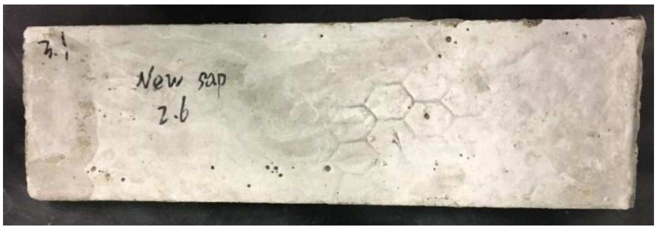

(b) After 100 cycles of wetting and drying

(c) After 50 cycles of freezing and thawing

Figure 72. Visual appearance of aerated slurry-infiltrated chicken mesh sheets subjected to different accelerated aging conditions.

Table 16. Flexural strength test results.

Accelerated Aging	Cyclic times	Flexural Strength, MPa
None	0	3.58 3.64 3.66
Wet-Dry Cycles	5	3.18 3.25 3.33
	50	3.16 3.22 3.28
	100	3.17 3.36
Freeze-Thaw Cycles	15	3.46 3.33 3.49 3.45
	50	2.99 3.11 3.23 3.08

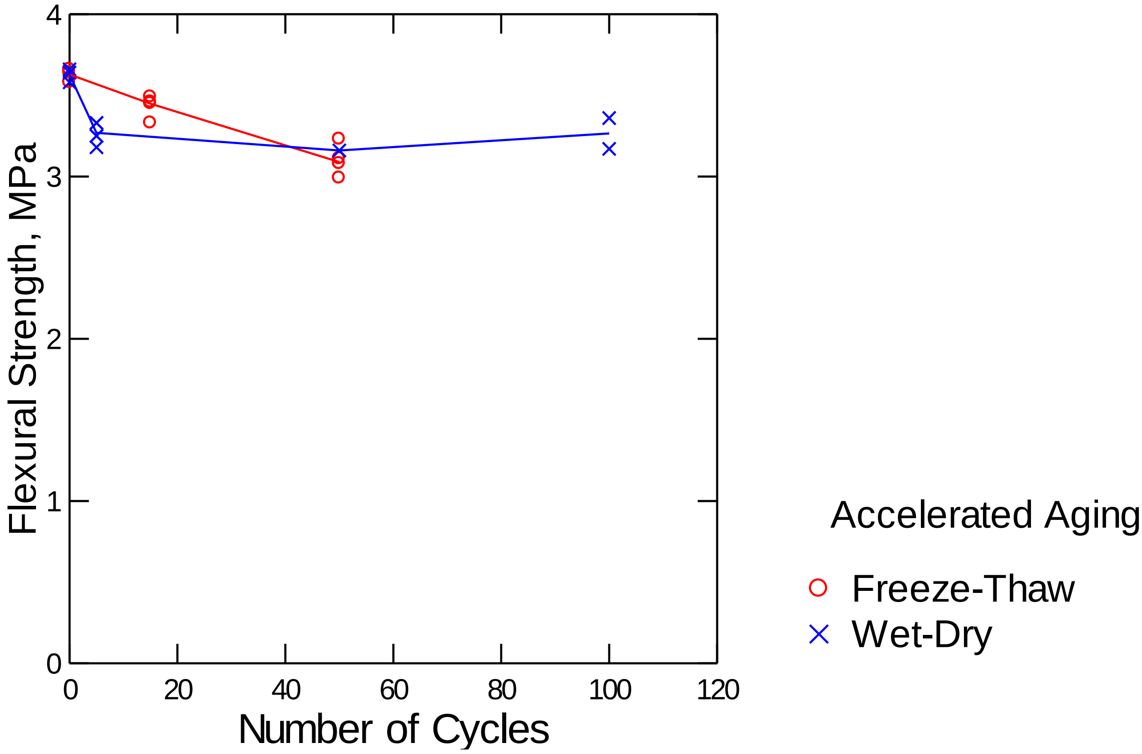

Figure 73. Flexural strength test results.

One potential concern with cementitious composites subjected to weathering effects relates to their embrittlement over time. Figure *74* and Figure *75* show the effects of repeated wet-dry and freeze-thaw cycles, respectively, on the flexural load-deflection behavior of the aerated slurry-infiltrated chicken mesh sheets. The ductility and energy absorption capacity (represented by the area underneath the flexural load-deflection curves) are observed to be retained under accelerated aging effects. Therefore, no trends towards embrittlement are observed under accelerated aging effects.

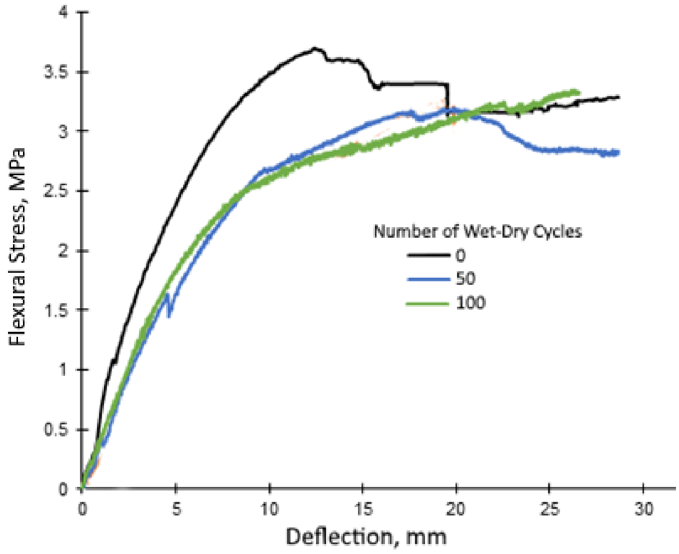

Figure 74. Effects of the number of wet-dry cycles on the flexural load-deflection behavior of aerated slurry-infiltrated chicken mesh sheets.

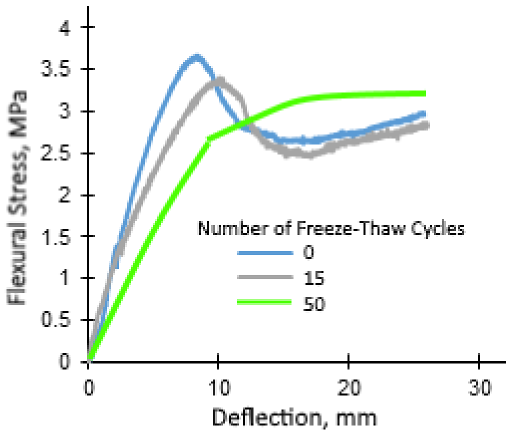

Figure 75. Effects of the number of freeze-thaw cycles on the flexural load-deflection behavior of aerated slurry-infiltrated chicken mesh sheets.

CHAPTER 8
CONCLUSIONS

Aerated slurry-infiltrated chicken mesh was developed as a lightweight building material which allows for construction of affordable, sustainable and safe building systems using locally available materials and resources. Screws are used for joining of aerated slurry-infiltrated chicken mesh structural components. Experimental investigations were conducted on the structural performance of specimens, structural elements and building components and screwed joints. The durability characteristics of aerated slurry-infiltrated chicken mesh sheets were also investigated. Structural analysis and design methods were developed for aerated slurry-infiltrated chicken mesh building system. A building structure was designed for full-scale construction and evaluation of its seismic performance. The conclusions derived at different phases of the project are presented below.

8.1. Mechanical Properties of Aerated Slurry-Infiltrated Chicken Mesh

1. The tensile behavior of aerated slurry-infiltrated chicken mesh relies upon the support provided by chicken mesh against realignment of the chicken mesh wires. This interaction depends on the quality (bearing capacity, elastic modulus and compressive strength) of the aerated slurry, and the concentration of chicken mesh as well as the specific surface area and the spacing of chicken mesh wires.
2. Slurry-infiltrated chicken mesh sheets exhibit a ductile behavior in tension. The transition from normal-density (non-aerated) slurry to aerated slurries of lower densities produces some drop in peak tensile load, but not in their ductile tensile load-deflection behavior. The tensile load-carrying capacity of aerated slurry-infiltrated chicken mesh does not increase proportionally

with the increasing number of chicken mesh layers per for the same sheet thickness. This is because it is the interaction between the chicken mesh with the aerated slurry that decides the ability to mobilize the chicken mesh load-bearing capacity within structurally viable deformations.

3. The aerated slurry-infiltrated chicken mesh sheets exhibit a distributed failure mode marked by crushing of the aerated slurry over a major fraction of the sheet volume. The crushing of aerated slurry when the aerated slurry-infiltrated chicken mesh sheet is subjected to tension further highlights the demand imposed by the tendency towards realignment of the chicken mesh wires under tension on the mechanical qualities of the aerated slurry.
4. The flexural load-deformation behavior of aerated slurry-infiltrated chicken mesh sheets was found to be exhibit qualitative similarities with their tensile behavior. The observations summarized above for tensile behavior also applies to flexural behavior.
5. The flexural failure mode of aerated slurry-infiltrated chicken mesh sheets is dominated by a single crack, and does not exhibit the distributed failure mode observed in tension. In spite of this, the flexural failure is still highly ductile. In the case of the selected aerated slurry with 0.8 g/cm^3 density, aerated slurry-infiltrated chicken mesh sheets with about 20 mm thickness would require about 12 layers of chicken mesh in order to reach viable levels of flexural strength.

8.2. Screw and Nail Behavior in Aerated Slurry-Infiltrated Chicken Mesh

6. An experimental investigation was conducted on the pullout behavior of screws or nails of different lengths and diameters from aerated slurry-infiltrated chicken mesh sheets of

different densities. An aerated slurry with maximum bulk density of 0.9 g/cm^3 could be nailed rather conveniently; a minimum nail diameter of 3-4 mm was found to be necessary in order to avoid buckling of the nail during application. The pullout behavior of nails and screws from aerated slurry-infiltrated chicken mesh sheets was ductile, and was not influenced consistently by the nail length and diameter within the narrow ranges of these variables considered in this investigation.

7. The number of chicken mesh layers in aerated slurry-infiltrated chicken mesh sheets had relatively small effects on the nail and screw pullout behavior. The bulk density of the aerated slurry, on the other hand, had notable effects on pullout behavior.
8. Screw or nail applied to aerated slurry-infiltrated chicken mesh sheets exhibit a highly ductile behavior with relatively high load-bearing capacity under monotonic lateral loads. This critical aspect of screw or nail behavior, which is relied upon in the indigenous building structure for dissipation of seismic energy input, was found to engage the chicken mesh layers. As the screw or nail lateral loading caused bearing failure of the aerated slurry, it started to engage and drag the chicken mesh layers; the pullout resistance of the chicken mesh embedded in aerated slurry was responsible for the relatively high lateral load-bearing capacity and the ductile behavior of screw or nail.
9. Cyclic lateral loading of screw or nail applied to aerated slurry-infiltrated chicken mesh sheets produced a pinched but stable hysteretic behavior with desired energy dissipation capacity. This was again attributed to the engagement of chicken mesh layers under cyclic lateral loading. The alignment of multiple screws or nails with respect to the loading direction was found to be an important factor influencing the hysteretic behavior under cyclic lateral loads. Alignment

of screws or nails perpendicular to the loading direction, which is relevant to the indigenous building systems considered here, produced a higher energy dissipation capacity by improving the stability of hysteretic curves produced at a constant deflection amplitude.

8.3. Behavior of a Lightweight Frame Made with Aerated Slurry-Infiltrated Chicken Mesh Under Cyclic Lateral Loading

10. An aerated slurry-infiltrated chicken mesh frame with column and beam cross-section comparable to those required for a single-story building design were subjected to cyclic lateral in-plane loading. The frame columns were fixed inside an aerated slurry-infiltrated chicken mesh footing. The frame failed by forming plastic hinges in beams near beam-column joints, which is compatible with the weak beam-strong column design of the frame.
11. The aerated slurry-infiltrated chicken mesh frame exhibited a ductile failure mode with a stable hysteretic behavior that provided significant energy absorption capacity.
12. The lateral load-bearing resistance, ductility and hysteretic energy absorption capacity of the aerated slurry-infiltrated chicken mesh frame were found to be favorable when compared with lateral load-resisting systems based on OSB and hardwood sheets.
13. The desired seismic performance of the aerated slurry-infiltrated chicken mesh frame can be attributed to the high specific surface area of chicken mesh, its desired mechanical interlocking within the cementitious matrix, its dual role as flexural and shear reinforcement, and the confining effects of the highly distributed chicken mesh reinforcement on the aerated slurry

matrix.

8.4. Structural Evaluation of a Lightweight Building System Made with Locally Available Materials

14. Aerated slurry-infiltrated sheets exhibit a ductile behavior under out-of-plane loading, which involves a somewhat distributed failure region.
15. Aerated slurry-infiltrated chicken mesh beams exhibited a highly ductile failure involving multiple cracking along an extended fraction of the beam length. The multiple cracks were spaced closely, and the aerated slurry within the failed region exhibited signs of both cracking and crushing, which could have been caused by the bearing action of the chicken mesh wires against the aerated slurry. Reversed loading of a beam after initial failure in the original direction produced a highly ductile behavior with a peak load that approached that in the original loading direction. This finding provides an initial indication of the desired hysteretic behavior of aerated slurry-infiltrated chicken mesh beams under cyclic loading.
16. Aerated slurry-infiltrated chicken mesh beams provided distinctly high levels of shear strength complemented with a ductile behavior in shear. These findings were explained by the dual role of flexural reinforcement that is distributed across the beam thickness as shear reinforcement, and also the highly ductile tensile behavior of aerated slurry-infiltrated chicken mesh. The high specific surface are of the chicken mesh reinforcement also benefits its dowel action against the aerated slurry.
17. Structural subcomponents comprising an aerated slurry-infiltrated chicken mesh frame to which aerated slurry-infiltrated chicken mesh sheets were nailed were tested under in-plane cyclic lateral loading. A frame without any sheets attached to it was also tested under similar

loading. Nailing of sheets increased the lateral load-bearing capacity of the frame by more than 50%. Both the frame tested alone and that tested with sheets nailed to it exhibited ductile behavior with desired energy dissipation capacity, with the hysteretic curves exhibiting a somewhat pinched attribute.

18. A structural subcomponent comprising two aerated slurry-infiltrated chicken mesh frames to which interior/exterior wall and ceiling/roof sheets were nailed was subjected to out-of-plane cyclic lateral loading. The behavior of this frame was governed by the bearing action of nails against the aerated slurry-infiltrated chicken mesh sheets. This subcomponent also provided a desired balance of strength, ductility and hysteretic energy absorption capacity, which could be attributed to the restraining effects of the chicken mesh layers against lateral movement of nails against aerated slurry-infiltrated chicken mesh sheets.

8.5. Structural Design of a Lightweight Building System Made with Locally Available Materials

19. The loads governing structural design of indigenous aerated slurry-infiltrated chicken mesh B-Huts were defined. Structural analyses were conducted in order to calculate the internal forces developed in different structural elements and (screwed) joints. The aerated slurry-infiltrated chicken mesh frames and (wall, roof/ceiling and floor sheets), and screws joining different sheets to frame elements were designed under the governing load combinations.
20. The aerated slurry-infiltrated chicken mesh structural frames and sheets designed for the building system had reasonable weights for manual handling and installation, noting that these elements tend to be somewhat heavier than the corresponding wood elements.

8.6. Durability Characteristics of Aerated Slurry-Infiltrated Chicken Mesh

21. Aerated slurry-infiltrated chicken mesh sheets provided stable behavior under two standard accelerated aging conditions designed for exterior cementitious roofing and siding building products. These accelerated aging conditions involved exposure to repeated cycles of wetting-drying and freezing-thawing. The flexural strength, ductility and energy absorption capacity of aerated slurry-infiltrated chicken mesh sheets were found to be stable under these accelerated aging conditions.

REFERENCES

REFERENCES

Abd-Elhamed, A. and S. Mahmoud (2017). "Nonlinear static analysis of reinforced concrete framed buildings-A case study on Cairo earthquake." Journal of Engineering Research **4**(4).

Abdullah, K., M. W. Hussin, F. Zakaria, R. Muhamad and Z. Abdul Hamid (2006). "POFA: A potential partial cement replacement material in aerated concrete."

Aboul-Anen, B., A. El-Shafey and M. El-Shami (2009). "Experimental and analytical model of ferrocement slabs." International Journal of Recent Trends in Engineering **1**(6): 25-29.

Ahmad, T., M. Arif and A. Masood (2014). "Experimental Investigations on Ferrocement Roof Slab System for Low Cost Housing." Journal of The Institution of Engineers (India): Series A **95**(1): 9-18.

Arroyo, O. and S. Gutiérrez (2016). "A seismic optimization procedure for reinforced concrete framed buildings based on eigenfrequency optimization." Engineering Optimization: 1-17.

ASTM (2012). Standard Test Methods for Mechanical Fasteners in Wood. **ASTM D1761:** 10.

Desayi, P. and V. Reddy (1991). "Strength of ligthweight ferrocement in flexure." Cement and Concrete Composites **13**(1): 13-20.

Dolan, J. (1994). "Proposed Test Method for Dynamic, Properties of Connections Assembled with Mechanical Fasteners." Journal of testing and evaluation **22**(6): 542-547.

Dolan, J. and A. Johnson (1996). "Cyclic tests of long shear walls with openings." Virginia Polytechnic Institute and State University, Timber Engineering Report No. TE-1996-002. Blacksburg, Virginia: VPISU.

Dolan, J. and B. Madsen (1992). "Monotonic and cyclic nail connection tests." Canadian Journal of Civil Engineering **19**(1): 97-104.

Dolan, J. D. and C. Heine (1997). Sequential phased displacement cyclic tests of wood-frame shear walls with various openings and base restraint configurations, Citeseer.

Dolan, J. D. and C. Heine (1997). Sequential phased displacement tests of wood-framed shear walls with corners, Virginia Polytechnic Institute and State University.

Ganne-Chedeville, C., A. Pizzi, A. Thomas, J. Leban, J.-F. Bocquet, A. Despres and H. Mansouri (2005). "Parameter interactions in two-block welding and the wood nail concept in wood dowel welding." Journal of adhesion science and technology **19**(13-14): 1157-1174.

Gatto, K. and C.-M. Uang (2003). "Effects of loading protocol on the cyclic response of woodframe shearwalls." Journal of Structural engineering **129**(10): 1384-1393.

Guandalini, S., O. L. Burdet and A. Muttoni (2009). "Punching tests of slabs with low reinforcement ratios." ACI Structural Journal **106**(1): 87.

Guo, M., Q. Juan, P. Li and Q. Yao (2011). "Seismic performance experimental research for multi-ribbed composite wall strengthened with aerated concrete blocks." Journal of Sichuan University: Engineering Science Edition **43**(1): 51-57.

He, M., F. Lam and H. G. Prion (1998). "Influence of cyclic test protocols on performance of wood-based shear walls." Canadian Journal of Civil Engineering **25**(3): 539-550.

Heinzmann, D., S. Etter, S. Villiger and T. Jaeger (2012). "Punching tests on reinforced concrete slabs with and without shear reinforcement." ACI Structural Journal **109**(6): 787.

Herzog, B. and B. Yeh (2006). Nail withdrawal and pull-through strength of structural-use panels. Proceedings of the 9 th World Conference on Timber Engineering.

Ibarra, L. F., R. A. Medina and H. Krawinkler (2005). "Hysteretic models that incorporate strength and stiffness deterioration." Earthquake engineering & structural dynamics **34**(12): 1489-1511.

Kazantzi, A. and D. Vamvatsikos (2012). "A study on the correlation between dissipated hysteretic energy and seismic performance." energy **30**(2): 2.2.

Kesner, K. E., S. L. Billington and K. S. Douglas (2003). "Cyclic response of highly ductile fiber-reinforced cement-based composites." ACI Materials Journal **100**(5): 381-390.

Krawinkler, H. (2009). Loading histories for cyclic tests in support of performance assessment of structural components. The 3rd international conference on advances in experimental structural engineering, San Francisco, Citeseer.

Memon, N. A., S. R. Sumadi and M. Ramli (2006). "Strength and Behaviour of Lightweight Ferrocement-Aerated Concrete Sandwich Blocks." Malaysian Journal of Civil Engineering **18**(2): 99-108.

Naaman, A. E. (2000). Ferrocement and laminated cementitious composites, Techno press.

Nambiar, E. K. and K. Ramamurthy (2007). "Air-void characterisation of foam concrete." Cement and concrete research **37**(2): 221-230.

Narayanan, N. and K. Ramamurthy (2000). "Structure and properties of aerated concrete: a review." Cement and Concrete Composites **22**(5): 321-329.

Ohsaki, M., T. Miyamura, M. Kohiyama, T. Yamashita and H. Akiba (2016). Seismic Response Simulation of Building Structures. High-Performance Computing for Structural Mechanics and Earthquake/Tsunami Engineering, Springer**:** 105-139.

Park, R. (1989). "Evaluation of ductility of structures and structural assemblages from laboratory testing." Bulletin of the New Zealand National Society for Earthquake Engineering **22**(3): 155-166.

Porter, M. L. (1987). Sequential phased displacement (SPD) procedure for TCCMAR testing. Proceedings of the Third Meeting of the Joint Technical Coordinating Committee on Masonry Research.

Ramamurthy, K., E. K. Nambiar and G. I. S. Ranjani (2009). "A classification of studies on properties of foam concrete." Cement and Concrete Composites **31**(6): 388-396.

Rose, J. D. (1998). Preliminary testing of wood structural panel shear walls under cyclic (reversed) loading, American Plywood Association.

Rosowsky, D. V. and T. A. Reinhold (1999). "Rate-of-load and duration-of-load effects for wood fasteners." Journal of Structural Engineering **125**(7): 719-724.

Ruiz-García, J. and J. D. Aguilar (2017). "Influence of modeling assumptions and aftershock hazard level in the seismic response of post-mainshock steel framed buildings." Engineering Structures **140**: 437-446.

Salenikovich, A. J. (2000). The racking performance of light-frame shear walls, Virginia Tech.

Salenikovich, A. J., J. D. Dolan and W. S. Easterling (1999). "Monotonic and cyclic tests of long steel-frame shear walls with openings."

Salonikios, T. N., A. J. Kappos, I. A. Tegos and G. G. Penelis (2000). "Cyclic load behavior of low-slenderness reinforced concrete walls: failure modes, strength and deformation analysis, and design implications." ACI Structural Journal **97**(1): 132-141.

Soudki, K. A., J. S. West, S. H. Rizkalla and B. Blackett (1996). "Horizontal connections for precast concrete shear wall panels under cyclic shear loading." PCI journal **41**(3): 64-80.

Sreevidya, V., R. Anuradha and R. Venkatasubramani (2012). "Experimental study on geopolymer ferro cement slab using various wire meshes." Journal of Structural Engineering (India) **39**(4): 436-443.

Thomsen IV, J. H. and J. W. Wallace (2004). "Displacement-based design of slender reinforced concrete structural walls—experimental verification." Journal of Structural Engineering **130**(4): 618-630.

Toothman, A. J. (2003). Monotonic and cyclic performance of light-frame shear walls with various sheathing materials, Virginia Polytechnic Institute and State University.

Uang, C. M. and V. V. Bertero (1990). "Evaluation of seismic energy in structures." Earthquake Engineering & Structural Dynamics **19**(1): 77-90.

Wafa, M. A. and K. Fukuzawa (2010). "Characteristics of ferrocement thin composite elements using various reinforcement meshes in flexure." Journal of Reinforced Plastics and Composites **29**(23): 3530-3539.

Zhang, Z., J. L. Provis, A. Reid and H. Wang (2014). "Geopolymer foam concrete: an emerging material for sustainable construction." Construction and Building Materials **56**: 113-127.